**Key Points:**
- The area at and around OmanDP Hole BT1B preserves nearly flat-lying tectonic "stratigraphy" of the basal thrust of the Samail ophiolite
- Recycling of $CO_2$ from subducting sediment into the mantle wedge produced listvenites (carbonated peridotite) at <200°C
- Subduction beneath the ophiolite was accommodated, in part, by ductile deformation of serpentinite and listvenite at <200°C

**Supporting Information:**
Supporting Information may be found in the online version of this article.

**Correspondence to:**
P. B. Kelemen,
peterk@LDEO.columbia.edu

# Listvenite Formation During Mass Transfer into the Leading Edge of the Mantle Wedge: Initial Results from Oman Drilling Project Hole BT1B

Peter B. Kelemen[1] ⓘ, Juan Carlos de Obeso[2] ⓘ, James A. Leong[1], Marguerite Godard[3] ⓘ, Keishi Okazaki[4] ⓘ, Alissa J. Kotowski[5] ⓘ, Craig E. Manning[6], Eric T. Ellison[7] ⓘ, Manuel D. Menzel[8] ⓘ, Janos L. Urai[8] ⓘ, Greg Hirth[9], Matthew Rioux[10] ⓘ, Daniel F. Stockli[11] ⓘ, Romain Lafay[3] ⓘ, Andreas M. Beinlich[12] ⓘ, Jude A. Coggon[13], Nehal H. Warsi[14], Jürg M. Matter[13] ⓘ, Damon A. H. Teagle[13] ⓘ, Michelle Harris[15] ⓘ, Katsuyoshi Michibayashi[16], Eiichi Takazawa[17], Zaher Al Sulaimani[18], and The Oman Drilling Project Science Team[19]

[1]Lamont Doherty Earth Observatory, Columbia University, Palisades, NY, USA, [2]Department of Geosciences, University of Calgary, Calgary, AB, Canada, [3]Géosciences Montpellier, Université de Montpellier, CNRS, Montpellier, France, [4]Kochi Institute for Core Sample Research, JAMSTEC, Kochi, India, [5]Department of Earth & Planetary Sciences, McGill University, Montreal, QC, Canada, [6]Department of Earth, Planetary & Space Sciences, University of California, Los Angeles, CA, USA, [7]Department of Geological Sciences, University of Colorado, Boulder, CO, USA, [8]Tectonics & Geodynamics, RWTH Aachen University, Aachen, Germany, [9]Department of Earth, Environmental and Planetary Sciences, Brown University, Providence, RI, USA, [10]Department of Earth Science, University of California, Santa Barbara, CA, USA, [11]Department of Geological Sciences, University of Texas, Austin, TX, USA, [12]Department of Earth Science, University of Bergen, Bergen, Norway, [13]Department of Ocean & Earth Science, National Oceanography Centre Southampton, Southampton, UK, [14]Alara Resources Ltd., Muscat, Oman, [15]School of Geography, Earth and Environmental Sciences, University of Plymouth, Plymouth, UK, [16]Department of Earth & Planetary Sciences, Nagoya University, Nagoya, Japan, [17]Department of Geology, Niigata University & VERC IMG JAMSTEC, Niigata, Japan, [18]Oman Water Society & Middle East Desalination Research Center, Muscat, Oman, [19]See Appendix A

**Abstract** This paper provides an overview of research on core from Oman Drilling Project Hole BT1B and the surrounding area, plus new data and calculations, constraining processes in the Tethyan subduction zone beneath the Samail ophiolite. The area is underlain by gently dipping, broadly folded layers of allochthonous Hawasina pelagic sediments, the metamorphic sole of the Samail ophiolite, and Banded Unit peridotites at the base of the Samail mantle section. Despite reactivation of some faults during uplift of the Jebel Akdar and Saih Hatat domes, the area preserves the tectonic "stratigraphy" of the Cretaceous subduction zone. Gently dipping listvenite bands, parallel to peridotite banding and to contacts between the peridotite and the metamorphic sole, replace peridotite at and near the basal thrust. Listvenites formed at less than 200°C and (poorly constrained) depths of 25–40 km by reaction with $CO_2$-rich, aqueous fluids migrating from greater depths, derived from devolatilization of subducting sediments analogous to clastic sediments in the Hawasina Formation, at 400°–500°. Such processes could form important reservoirs for subducted $CO_2$. Listvenite formation was accompanied by ductile deformation of serpentinites and listvenites—perhaps facilitated by fluid-rock reaction—in a process that could lead to aseismic subduction in some regions. Addition of $H_2O$ and $CO_2$ to the mantle wedge, forming serpentinites and listvenites, caused large increases in the solid mass and volume of the rocks. This may have been accommodated by fractures formed as a result of volume changes, mainly at a serpentinization front.

**Plain Language Summary** This paper reports initial results from study of core from Oman Drilling Project Hole BT1B and the surrounding area. It provides insights into subduction zone processes, including large fluxes of recycled $CO_2$ from subducting sediments into the leading edge of the mantle wedge, and surprisingly low temperature ductile deformation at less than 200°C. Recycling of $CO_2$ via carbon mineralization in the hanging wall of subduction zones may produce an important, lithospheric reservoir in the global carbon cycle. Ductile deformation of serpentinite, and during or after transformation of peridotite to listvenites (mixtures of carbonates and opal or quartz) could explain aseismic subduction atop some subduction zones.

**Investigation:** Peter B. Kelemen, Juan Carlos de Obeso, James A. Leong, Marguerite Godard, Keishi Okazaki, Alissa J. Kotowski, Craig E. Manning, Eric T. Ellison, Manuel D. Menzel, Janos L. Urai, Greg Hirth, Matthew Rioux, Daniel F. Stockli, Romain Lafay, Andreas M. Beinlich, Jude A. Coggon

**Methodology:** Peter B. Kelemen, Juan Carlos de Obeso, James A. Leong, Marguerite Godard, Keishi Okazaki, Craig E. Manning, Eric T. Ellison, Manuel D. Menzel, Matthew Rioux, Daniel F. Stockli

**Project Administration:** Peter B. Kelemen, Jude A. Coggon, Nehal H. Warsi, Jürg M. Matter, Damon A. H. Teagle, Michelle Harris, Katsuyoshi Michibayashi, Eiichi Takazawa, Zaher Al Sulaimani

**Supervision:** Peter B. Kelemen, Janos L. Urai, Jude A. Coggon, Nehal H. Warsi, Jürg M. Matter, Damon A. H. Teagle, Michelle Harris, Katsuyoshi Michibayashi, Eiichi Takazawa

**Visualization:** Peter B. Kelemen, James A. Leong, Marguerite Godard, Keishi Okazaki, Craig E. Manning, Eric T. Ellison

**Writing – original draft:** Peter B. Kelemen, Juan Carlos de Obeso, James A. Leong

**Writing – review & editing:** Peter B. Kelemen

## 1. Introduction

Oman Drilling Project (OmanDP) Hole BT1B at 23.364374°N, 58.182693°E, about 12 km southeast of the town of Fanjah in the Sultanate of Oman, sampled serpentinized peridotites and listvenites (fully carbonated peridotites, Halls & Zhao, 1995) at the base of the Samail ophiolite, the basal fault of the ophiolite, and the underlying metamorphic sole, with the intention of investigating mass transfer and deformation in the leading edge of the mantle wedg overlying a Tethyan subduction zone. Study of outcrops along the contact between the sole and the peridotite can illuminate processes in and above a subduction zone that are generally inaccessible to direct observation. Of particular interest are (a) the source of footwall fluids, (b) the nature and mechanism of fluid transport along the thrust fault and into the mantle wedge, (c) chemical, mineralogical and rheological modification of the hanging wall by reaction with footwall fluids, and (d) the mechanisms of subduction zone deformation.

Hole BT1B was drilled using cylindrical diamond bits and wireline core retrieval, from March 7 to 23 March 2017. Core recovery was ~100% throughout the Hole. Core was shipped to Japan and loaded onto Drilling Vessel Chikyu, where the OmanDP Science Team performed analyses closely following protocols established by the various incarnations of the Ocean Drilling Program (currently, the International Ocean Discovery Program, IODP). Detailed core descriptions, together with drilling history and some background information (Kelemen, Matter, et al., 2020) are available online at http://publications.iodp.org/other/Oman/VOLUME/CHAPTERS/113_BT1.PDF

This paper reports new mapping and structural observations, mineral analyses and modeling, together with a summary of prior observations. It is intended to provide interpretive context for more detailed studies of core from Hole BT1B and the geology of the surrounding region. Such studies in this Special Issue of the Journal of Geophysical Research include those focused on textural and petrologic data for listvenites (Beinlich et al., 2020; Lafay et al., 2020) and the metamorphic sole (Kotowski et al., 2021), volume changes during serpentinization (Malvoisin et al., 2020), major and trace element geochemistry with relevance to subduction zone mass transfer (Godard et al., 2021; Okazaki et al., 2021), Mg-, Sr- and C-isotope geochemistry constraining the source of $CO_2$-bearing fluids and the fluid-rock reaction process (de Obeso, Kelemen, et al., 2022; de Obeso, Santiago Ramos, et al., 2021) and deformation of the listvenites (Menzel et al., 2020, 2021).

Section 2 provides geological context for observations of core and surrounding outcrops. Section 3 summarizes methods used to produce results presented for the first time in this paper. Section 4 reports new geological field observations and analytical data, and reviews key results from Kelemen, Matter, et al. (2020) in context. Section 5 discusses the pressure, temperature and timing of listvenite formation, the nature and source of the fluids that transformed mantle peridotite into serpentinite and listvenite, the chemical and mechanical processes during these transformations, and deformation of altered mantle peridotite immediately above a paleo-subduction zone beneath the leading edge of the mantle wedge.

It is hoped that this paper, and the other papers in this Special Issue, will provide a starting point for future investigations of this unique and important site. In this context, readers should be aware that the archive half of the core is currently stored at Petroleum Development Oman where it is available for viewing, the working half of the core is stored at the American Museum of Natural History, where it can be sampled upon request to the Museum, and a huge volume of data from shipboard visual core observations and analytical data is available to anyone at http://publications.iodp.org/other/Oman/OmanDP.html, https://www.icdp-online.org/projects/world/asia/oman/, and other sites that can be accessed from there.

## 2. Geological Setting

### 2.1. Regional Geologic Context

The Samail ophiolite is composed of oceanic crust formed at a submarine spreading center above a subduction zone. The crustal thickness and composition of the ophiolite is similar to the geophysically and geologically constrained characteristics of fast-spreading, Pacific oceanic crust, with a few km of submarine lavas and sheeted dikes overlying a thicker, gabbroic lower crust (e.g., Christensen & Smewing, 1981; Coleman & Hopson, 1981; Nicolas et al., 1996) However, the lavas have a trace element "subduction signature" (Alabaster et al., 1982; Pearce & Peate, 1995; Pearce et al., 1981), and parental, mantle-derived magmas appear to have contained 0.2–2 wt% $H_2O$, substantially more than in primitive mid-ocean ridge basalts (MacLeod et al., 2013). Beneath the crustal

section of the ophiolite, residual mantle peridotites and tabular dunites record polybaric decompression melting, melt extraction, and focused transport of basaltic melt upward to form the crust (Braun & Kelemen, 2002; Godard et al., 2000; Kelemen et al., 1995, 2000; Monnier et al., 2006).

### 2.2. Lithologies at the Base of the Samail Ophiolite

Here we describe the units above and below the basal fault of the Samail ophiolite. We begin with a review of work on the metamorphic sole. Then, we describe the overlying Banded Unit at the base of the ophiolite's mantle section. Finally, we briefly outline the nature of the sedimentary rocks beneath the metamorphic sole.

Beneath the mantle section of the ophiolite, and above allochthonous sediments of the Hawasina Formation, are discontinuously exposed lenses of a "metamorphic sole". Peak pressures and temperatures in the sole generally record hot subduction conditions at temperatures up to 700°C–900°C (Cowan et al., 2014; Ghent & Stout, 1981; Hacker & Gnos, 1997; Searle & Cox, 1999, 2002; Searle & Malpas, 1980, 1982; Searle et al., 1980; Soret et al., 2017) though at BT1B peak temperatures are 450°C–550°C (Kotowski et al., 2021). Apparently—based on published data and calculations—the sole records a broad range of peak pressures from a possible lower limit of 200 MPa (Ghent & Stout, 1981) or 800 MPa (Soret et al., 2017) to a possible upper limit of 1400 MPa (Cowan et al., 2014; Searle & Cox, 2002). Kotowski et al. (2021) report that the sole in core from Hole BT1B records a peak pressure in the range of 800–1200 MPa.

The sole contains metasediments and meta-volcanic rocks—including submarine pillow lavas—with the major element compositions of mid-ocean ridge basalts (MORB) as well as alkali basalts and more evolved andesites and dacites (Alabaster et al., 1982; Ernewein et al., 1988; MacLeod et al., 2013; Pearce et al., 1981; Searle et al., 1980). In core from BT1B, alkaline metabasalt compositions in the sole (Godard et al., 2021; Kelemen, Matter, et al., 2020) are unlike the magmas that formed the crust of the Samail ophiolite. In the ophiolite, the structurally lowest, "Geotimes" or "V1" lavas are similar to normal mid-ocean ridge basalts, though they probably were hydrous and they contain a hint of an arc trace element signature (Alabaster et al., 1982; Ernewein et al., 1988; MacLeod et al., 2013; Pearce et al., 1981). Their composition, and that of dunite conduits for transport of primitive melts parental to V1 through the shallow mantle, is consistent with formation of the gabbroic lower crust in the Samail and Wadi Tayin massifs of the ophiolite from primitive V1 magmas (Braun & Kelemen, 2002; Kelemen et al., 1995, 1997). The overlying "Lasail" or "V2" lavas in the ophiolite are incompatible-element-depleted, with a stronger subduction signature (Alabaster et al., 1982; Ernewein et al., 1988; MacLeod et al., 2013; Pearce et al., 1981) and include boninites (e.g., Ishikawa et al., 2002) as well as tholeiitic basalts, andesites and dacites. Neither V1 nor V2 lavas are similar to the alkali basalt compositions in the sole. The present day $^{87}Sr/^{86}Sr$ ratios in the alkali basalts in core from BT1B range from 0.704 to 0.706 (de Obeso, Kelemen, et al., 2022), more radiogenic than MORB. Though their Sr isotope ratio may have been modified by alteration, one possibility is that the alkali basalts are remnants of subducted seamounts with elevated $^{87}Sr/^{86}Sr$, similar to accreted seamounts along the Cascadia margin of North America (e.g., Duncan, 1982).

In addition to metabasalts, regionally the sole contains metasediments, and "exotic limestones", all incorporated by Searle and Malpas (1980) in the "Haybi Formation". However, in this paper we informally group the Haybi Formation into an undifferentiated metamorphic sole unit. In the sole sampled by drill core from Hole BT1B, metasediments are clearly distinguishable from the metabasalts based on texture, but some of them are compositionally similar to the metabasalts, perhaps reflecting a volcanoclastic origin, whereas others grade into somewhat odd, low-$SiO_2$, muscovite-bearing lithologies (Godard et al., 2021; Kelemen, Matter, et al., 2020; Kotowski et al., 2021).

Above the sole—where it is present—and elsewhere at the base of the ophiolite, the lower few km of the mantle section contains easily visible, meter to 10-m scale, parallel bands of dunite, harzburgite and (rare) lherzolite, informally known as the Banded Unit (Godard et al., 2000; Khedr et al., 2013, 2014; Linckens et al., 2011; Lippard et al., 1986; Prigent, Agard, et al., 2018; Prigent, Guillot, et al., 2018; Takazawa et al., 2003; Yoshikawa et al., 2015). The lithological contacts in this unit are sharp. These contacts have low angle dips with respect to the paleo-seafloor, the crust-mantle transition zone, and the basal fault that juxtaposes mantle peridotite with the metamorphic sole. Mylonitic shear zones are present in the Banded Unit, with textures recording deformation at 700°C–1,000°C (Boudier et al., 1988; Herwegh et al., 2016; Linckens et al., 2011; Prigent, Agard, et al., 2018). Thus, there is evidence for high strain ductile deformation and transposition of layering at the base of

the mantle section, which might also have accommodated substantial thinning (Prigent, Agard, et al., 2018; Soret et al., 2017). Similarly, there is evidence for thinning of the units below the ophiolite (Grobe et al., 2018, 2019).

While some of the range in temperature and pressure estimates from the sole and the Banded Unit may be due to analytical and methodological uncertainty, or incomplete preservation and sampling of the highest-grade rocks, some may be due to temporal and spatial variability in peak metamorphic conditions. Moreover, the temperature record may be biased toward peak conditions, rather than later cooling. At the initiation of subduction near a spreading ridge, hot metamorphic rocks from the footwall may be accreted to the hot base of the newly formed mantle wedge, whereas as subduction zones grow colder and develop a steady-state thermal structure, cold dense lithologies in the footwall may be subducted (Agard et al., 2016; Soret et al., 2017). If so, the metamorphic sole in Oman may record the anomalously high temperatures of subduction initiation, and not the lower temperatures of evolution toward a steady-state subduction zone geotherm. The relatively low temperatures recorded by the sole in BT1B core could represent a point along this cooling path (Kotowski et al., 2021).

A close correspondence between 96 and 95 Ma igneous ages in the crust, and both $^{40}Ar/^{39}Ar$ and zircon U/Pb ages of metamorphic rocks along the basal thrust (ca. 96–94 Ma), indicates that thrusting of the Samail ophiolite over adjacent oceanic crust and nearby pelagic sedimentary units began during formation of igneous crust in the ophiolite (e.g., Garber et al., 2020; Hacker & Gnos, 1997; Hacker & Mosenfelder, 1996; Hacker et al., 1996; Rioux, Garber, et al., 2021; Rioux et al., 2012, 2013, 2016; Stanger, 1985; Styles et al., 2006; Tilton et al., 1981; Warren et al., 2005) or perhaps even earlier (Guilmette et al., 2018).

The base of the metamorphic sole is truncated by a fault contact with autochthonous, low-grade metasediments of the Hawasina Formation, composed of pelagic clastic units interlayered with limestones (Béchennec et al., 1988, 1990). Relatively high, age corrected $^{87}Sr/^{86}Sr$ ratios in the clastic units suggest that they are distal sediments derived from erosion of continental crust (de Obeso, Kelemen, et al., 2022; Weyhenmeyer, 2000), while carbonate units record Sr isotope ratios similar to those of Mesozoic seawater (Weyhenmeyer, 2000; Wohlwend et al., 2017). These sedimentary units were thrust over Mesozoic to Proterozoic rocks of the Arabian continental margin, forming a "rumpled rug" between the autochthon and the ophiolite throughout northern Oman and the eastern United Arab Emirates.

### 2.3. History of the Basal Thrust of the Samail Ophiolite

Where the metamorphic sole is preserved, its tectonic contact with the mantle section of the ophiolite represents a paleo-subduction zone at the base of the ophiolite, which consumed several hundred kilometers of Tethyan basin and then continental crust before coming to rest on the Arabian continental margin (Béchennec et al., 1988, 1990; Breton et al., 2004; Cooper, 1988; Ninkabou et al., 2021; Robertson & Searle, 1990; van Hinsbergen et al., 2019). During this time, the overlying peridotite was "the leading edge of the mantle wedge".

During coeval metamorphism of the sole and igneous accretion of the crust in the ophiolite, the relative locations of these two units are uncertain. Primitive V1 magmas in the ophiolite, with compositions almost indistinguishable from mid-ocean ridge basalts (MORB), crystallized to form most of the crust, particularly in the southern Wadi Tayin and Samail massifs that were the site of the OmanDP boreholes. Like MORB worldwide, these magmas probably formed via polybaric decompression melting over a depth interval of 75 km or more (e.g., Allegre et al., 1973; Asimow et al., 2004; Bottinga & Allegre, 1973; E. M. Klein & Langmuir, 1987; McKenzie & Bickle, 1988). Thus, the metamorphic sole (recording peak depths less than 40 km) must not have been directly beneath the spreading center during crustal formation and metamorphism. Instead, the ophiolite section and the metamorphic sole were juxtaposed after crust formation and after peak metamorphism in the sole.

Moreover, the structural thickness of the Samail ophiolite measured perpendicular to the paleo-seafloor and/ or the crust/mantle transition zone, and including both crust and mantle sections, never exceeds ∼20–30 km (Boudier & Coleman, 1981; Nicolas et al., 2000), corresponding to a pressure less than or equal to ∼800 MPa, beneath ∼7 km of crust (on average, Nicolas et al., 1996) and up to ∼20 km of fresh mantle peridotite. Thus, the structural thickness of the ophiolite appears to be at least 10 km less than the depth inferred from the high end of the pressure range recorded by the sole (1300 or 1400 MPa, ∼ 40–45 km). In addition, there is no evidence for widespread, tectonic thinning of the crustal section of the ophiolite, either by faulting or ductile deformation.

How can these data be reconciled? One possibility is that the peak pressures inferred for the sole are imprecise, and/or that they represent tectonic "overpressures" that don't correspond closely with depth (Garber et al., 2020). In this interpretation, the metamorphism of the sole could have occurred at ~800 MPa, corresponding to the current structural thickness of the ophiolite. A second possibility, as noted above, is that the base of the mantle section of the ophiolite underwent tectonic thinning, perhaps via transpression (Prigent, Agard, et al., 2018; Soret et al., 2017). A third alternative is that some of the lenses of the metamorphic sole—those recording the highest pressures—migrated updip to reach their current structural position, ~25 km below the paleo seafloor. Indeed, upward transport of buoyant footwall lithologies during subduction is recorded in many preserved collisional orogens (e.g., Chemenda et al., 2000). If so, updip migration of the sole with respect to the overlying ophiolite must have occurred after peak metamorphism but during Tethyan subduction, prior to emplacement of the ophiolite and the sole over the allochthonous Hawasina sediments. Finally, of course, it is possible that the current juxtaposition of the sole and the base of the ophiolite may be explained as the result of combinations of these three alternatives.

Subsequent events have affected the wedge, the sole, the underlying sedimentary units, and the faults between them (Grobe et al., 2018, 2019). The end of subduction and emplacement of the ophiolite over allochthonous Hawasina sediments and the autochthonous, Arabian continental margin was followed by subaerial erosion, and then by a marine transgression marked by deposition of shallow water limestones at ~74 Ma (Al Khirbash, 2015; Alsharan & Nasir, 1996; Bailey, 1981; Hansman et al., 2017; Nolan et al., 1990; Schlüter et al., 2008; Wyns et al., 1992). Then, large scale uplift deformed all these units, forming the gigantic Jebel Akdar and Saih Hatat domes, cored by Proterozoic continental crust (e.g., Glennie et al., 1973, 1974). Saih Hatat uplift and cooling started at about 60 Ma, if not earlier (e.g., Grobe et al., 2018, 2019; Hansman et al., 2017). Doming reactivated and cut the basal thrust of the ophiolite in normal faults and shear zones. Some of these younger faults juxtaposed mantle peridotite from the ophiolite with the allochthonous Hawasina sedimentary rocks, and even with the autochthonous platform carbonates of the Arabian continental margin, along tectonic contacts where the metamorphic sole is no longer present.

However, despite these complexities, we reiterate that—where it is parallel to banding and foliation—the contact between the metamorphic sole and the overlying Banded Unit at the base of the Samail ophiolite mantle section represents the basal thrust of the ophiolite. In this paper, when we refer to the "basal thrust", we are referring to contacts that preserve these characteristics. In turn, though of course there can have been imbrication and/or subduction erosion, the basal thrust of the ophiolite represents the locus of 100's of kilometers of subduction of oceanic crust, overlying sediments and, ultimately, the Arabian continental margin.

### 2.4. Geology of MoD Mountain

Hole BT1B is on the north side of the wide Wadi Mansah, southeast of "Ministry of Defense Mountain", (MoD Mountain), which is informally named for the military firing range on the south side of Wadi Mansah. The MoD Mountain region is close to the saddle between the northeastward plunging end of the Jebel Akdar massif, to the west, and the westward plunging Saih Hatat massif to the northeast (Figure 1).

This region preserves a gently folded, tectonic "stratigraphy" (Figures 2, 3, and 4). The lowest exposed units in this sequence, northeast of Hole BT1B, are diagenetically-altered sedimentary rocks, mostly clastic shales and slates with a few meter to 10 m scale intercalations of limestone and minor lenses of metavolcanic rocks. These are parts of the Hawasina Formation (Béchennec et al., 1988, 1990). Overlying the Hawasina Formation is one of the most aerially extensive outcrops of the metamorphic sole in Oman and the UAE (e.g., Figure 1 and geologic maps in Soret et al., 2017; Wilde et al., 2002). The outcrop area is unusually large in this region because the unit is regionally flat lying, though broadly folded.

Above the metamorphic sole in this gently folded "stratigraphy" is partially serpentinized peridotite, composed of distinctive, banded alternations of dunite, harzburgite and lherzolite on a scale of meters to tens of meters, characteristic of the "Banded Unit" at the base of the ophiolite (Boudier & Coleman, 1981; Boudier et al., 1988; Lippard et al., 1986; Searle & Cox, 2002). Indeed, partially serpentinized mantle peridotites on MoD Mountain, northeast of Hole BT1B have compositions similar to the Banded Unit elsewhere, and distinct from shallower, residual mantle peridotites of the Samail ophiolite section, as discussed in Section 5.5, below. The presence of
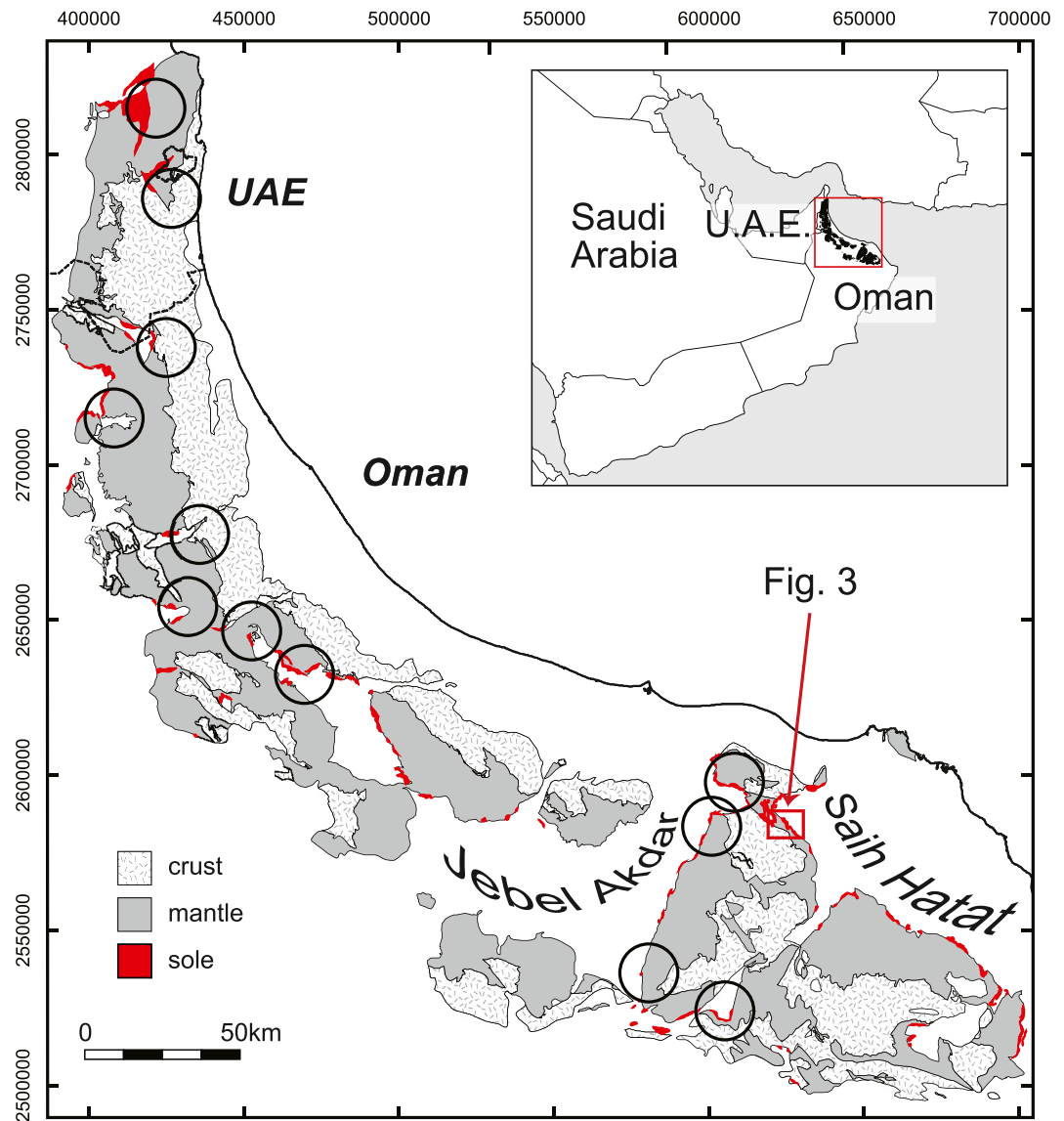
**Figure 1.** Outcrop area of the Samail ophiolite in Oman and the UAE, based on Nicolas et al. (2000). Metamorphic sole, in red. Black circles indicate approximate location of listvenites (Nasir et al., 2007; Stanger, 1985; Wilde et al., 2002). Red rectangle indicates the approximate location of Figures 3 and 4, geologic maps of the site of OmanDP Hole BT1B and vicinity.

the Banded Unit overlying the metamorphic sole is another indication that MoD Mountain area exposes the basal thrust of the ophiolite—the paleo-subduction zone—together with the overlying mantle wedge.

In some localities, peridotites at the base of the Samail ophiolite mantle section have undergone 100% carbonation at ~100°C–200°C to form "listvenites" (Beinlich et al., 2020; Falk & Kelemen, 2015; Glennie et al., 1974; Lafay et al., 2020; Nasir et al., 2007; Stanger, 1985; Wilde et al., 2002), in which all Mg and Ca are in carbonate minerals, and silica derived from olivine and pyroxene has formed quartz or chalcedony. In Oman, such listvenites are most abundant on and around MoD Mountain northeast of Hole BT1B, where they form part of the gently folded tectonic "stratigraphy" we are discussing here. Listvenites on the flanks of MoD Mountain form discontinuous tabular lenses with low angle dips, 10–200 m thick, parallel to the basal thrust and to lithological banding in the peridotite (Figure 2). These lenses occur along the basal thrust—between peridotite and the sole—and enclosed within the peridotite, up to 300 m above the sole. Over the years, workers have speculated informally

**Figure 2.** Photograph of the west end of the MoD Mountain ridge, from the SW, looking NE, showing bands of listvenite (rusty orange) parallel to contacts between partially serpentinized harzburgite (brown) and dunite (tan) comprising the "Banded Unit" at the base of the Samail ophiolite mantle section. Greenish metabasalts and metasediments of the metamorphic sole underlying the ophiolite are exposed along indistinct ridge in lower left. The listvenite band at top right is more than 100 m thick and extends for 1.5 km along the length of the summit ridge. The listvenite band in the center of the photo is 15–20 m thick. Photo taken with a telephoto lens from ~23.35°N, 58.17°E, along azimuth ~030°.

that the bands above the basal thrust formed along permeable pathways created by imbricate thrust faults in the peridotite. Contacts in outcrop between listvenite and the surrounding, partially serpentinized peridotite are marked by strongly foliated, 100% serpentinized zones, 1 to >20 m thick.
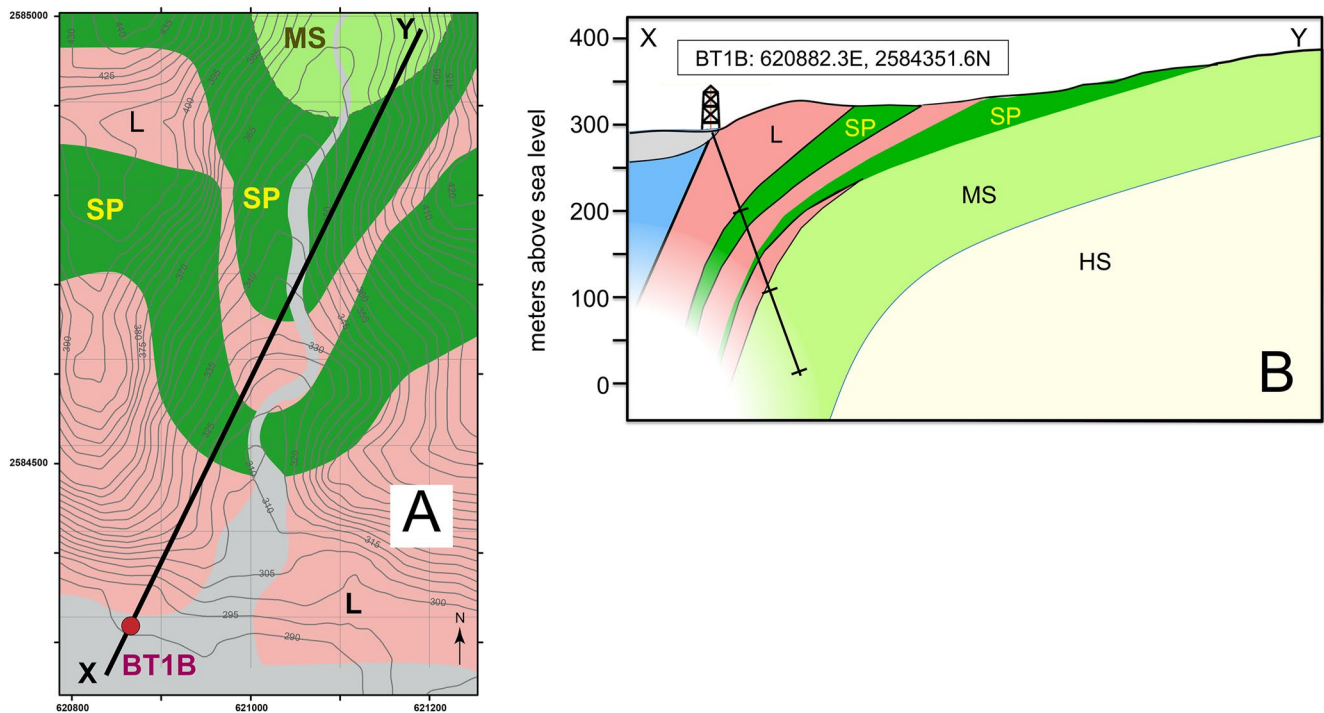


**Figure 3.** Map and cross section of the area NNE of Oman Drilling Project Site BT1. Yellow, HS: Hawasina sediments; light green, MS: metamorphic sole; rusty red, L: listvenite; dark green, SP: serpentinized peridotite; blue: inferred gabbro, based on outcrops south of Wadi Mansah; gray: gravels of Wadi Mansah. UTM coordinates in meters. Cross section has no vertical exaggeration. Map and cross-section modified from Figures F1 and F2 in Kelemen, Matter, et al. (2020).
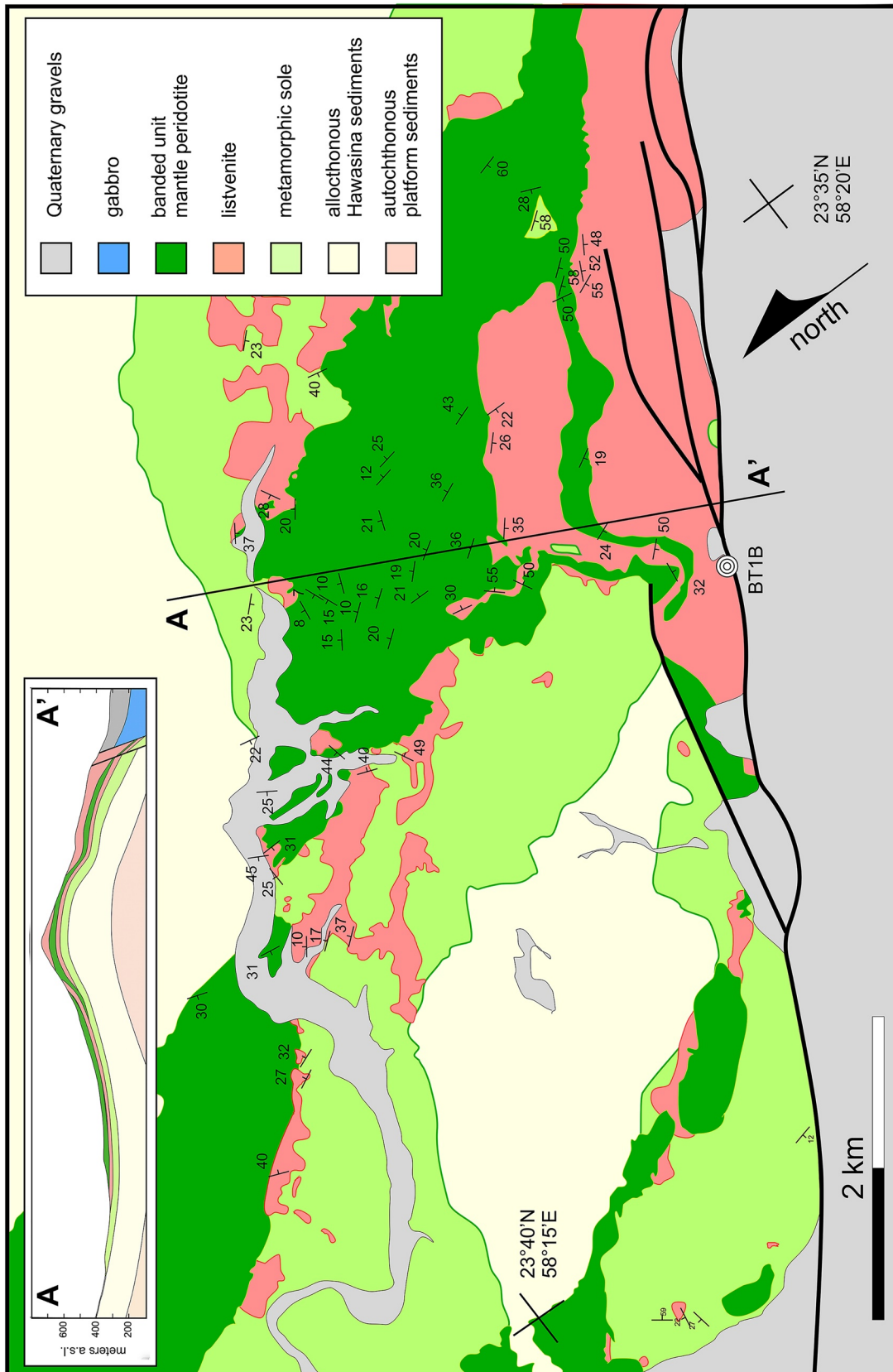
**Figure 4.**

The lithological banding in the peridotite and the listvenite lenses dip gently south on the south side of MoD Mountain, north on the north slopes of the mountain, and then south again along and NE of the wadi bounding MoD Mountain to the north (Falk & Kelemen, 2015 and this paper, Section 4.2). Despite later faulting, these structures define a broad anticline with an axis approximately coincident with the summit ridge of MoD Mountain, and a syncline with an axis roughly coincident with the wadi northeast of MoD Mountain. Listvenites form erosion resistant dip slopes and the tops of small buttes outlining the folded stratigraphy.

Listvenites elsewhere in Oman and the UAE are found along the basal thrust, commonly juxtaposed with, or within a few km of, the metamorphic sole and/or the Banded Unit at the base of the Samail mantle section (e.g., Glennie et al., 1974), as at MoD Mountain. In some other outcrops, listvenites form lenses within broad serpentinite mélange zones at the base of the ophiolite (Nasir et al., 2007; Stanger, 1985). In contrast, listvenites are not found within the peridotite more than a few kilometers away from the basal thrust of the ophiolite.

A Rb/Sr isochron on listvenite mineral separates (97 Ma $\pm$ 29 Ma 2$\sigma$, Falk & Kelemen, 2015) is similar to the better determined 96 to 94 Ma U/Pb ages of zircon in the metamorphic sole and igneous crust in the ophiolite. Based on the listvenite mineral isochron, there is a 67% probability that the listvenites are older than 82.5 Ma (average – 1$\sigma$), and a 93% probability that they are older than 75 Ma (1.5$\sigma$), before the end of subduction. Thus, geological observations (summarized above and in Section 4.2) together with the isochron data indicate that the listvenites formed via transfer of $CO_2$ and other components derived from subducting material—probably sediments and/or altered lavas—into the leading edge of the mantle wedg during Tethyan subduction and ophiolite emplacement. New geological data supporting this are presented in 4.2. Sections 5.6 and 5.7 provide thermodynamic modeling that quantifies this hypothesis.

As noted in Section 2.4, Paleocene to Miocene uplift of the nearby Jebel Akdar and Saih Hatat massifs may have caused reactivation of some older faults, and definitely formed new, younger faults in the MoD area. For example, shallow-level gabbros and sheeted dikes are juxtaposed with mantle peridotite and the metamorphic sole on a steep fault parallel to Wadi Mansah, just south of Hole BT1B (Villey et al., 1986; Wilde et al., 2002). In another possible example, Scharf et al. (2020) report early U/Pb formation or cooling ages (60 $\pm$ 16 and 58 $\pm$ 6 Ma) of calcite veins that cut listvenite, cataclasite and fault contacts between listvenite and post-emplacement, Late Cretaceous conglomerates.

## 3. Methods

Here we describe methods used for new data presented for the first time in this paper. Section S2 in Supporting Information S1 provides methods for data illustrated in this paper, but previously reported elsewhere.

### 3.1. Geological Mapping

Geological field work to produce the map and cross-section in Figure 4 spanned short visits over about a decade. Contacts and structural measurements were located by GPS at the time of measurement. The topographic profile for the cross section was constructed using Google Earth.

### 3.2. Raman Spectroscopy

Analyses of minerals in thin section and rock slabs were conducted at the Raman Microspectroscopy Laboratory, University of Colorado-Boulder with a Horiba Scientific LabRam HR Evolution Raman microscope. Measurements used a 100 mW 532 nm laser, focused through a 50× (0.75 NA) microscope objective onto a ~2 µm spot. The laser power was modulated with neutral density filters to about 15 mW at the sample surface. Multiple (2–10) accumulations were coadded in order to filter spikes and improve signal to noise, and the acquisition time and accumulation number were adjusted to yield appropriate data quality. Data processing was performed using

**Figure 4.** Geologic map and cross section of MoD Mountain and vicinity. Complex map pattern arises from intersection of topography with broadly folded, gently dipping units, as is more evident in the cross section (no vertical exaggeration) illustrating the antiform coinciding with MoD Mountain, and the syncline to its north. Dips are all measured on lithologic contacts, including dunite/harzburgite contacts within the Samail ophiolite mantle section.

LabSpec 6 software (Horiba Scientific), including correction for instrumental artifacts and polynomial baseline fitting/subtraction. Raman mapping was performed using a motorized stage with 2 μm step size, and map datasets were fit using classical least-squares fitting with endmember spectra isolated from regions within the map using LabSpec 6 after data processing.

### 3.3. Thermodynamic Calculations and Modeling

The speciation and chemical mass transfer code EQ3/6 (Wolery, 1992) was used to predict the compositions of coexisting solid and aqueous phases that evolved during interaction between representative lithologies from the MoD Mountain area and $CO_2$-bearing fluids. Thermodynamic data for minerals were mostly from Berman (1988). Data for pyrite and pyrrhotite were from Helgeson et al. (1978). For aqueous species, thermodynamic data used in the simulations were calculated using the Deep Earth Water (DEW) model (Huang & Sverjensky, 2019; Sverjensky et al., 2014) which uses recent experimental and theoretical advances (Facq et al., 2016; Pan et al., 2013) to expand the extended Helgeson-Kirkham-Flowers (HKF) aqueous equation of state (Shock et al., 1992, 1997) to pressures up to 6.0 GPa.

The compositions of 5 wt% aqueous fluid in equilibrium with pelitic and carbonate-bearing lithologies from the Hawasina Formation at 400°C–700°C and 0.5–2.0 GPa were calculated. For example, a dilute fluid was equilibrated with the rock composition of sample OM20-17 (de Obeso, Kelemen, et al., 2022), containing 0.06 wt% total carbon (Table S2 in Supporting Information S1). The CaO content of OM20-17 was below detection. For the model calculations it was assumed to be 0.1 wt%. In addition, the S content of this sample has not been measured. For this calculation it was assumed to be 100 ppm. At these high temperatures, carbonate minerals are unstable in pelitic and mixed clastic + carbonate lithologies, and most of the carbon in these rocks will be mobilized into the fluid phase as dissolved $CO_2$.

We calculated the outcome of cooling of the calculated, initial $CO_2$-rich fluid in equilibrium with OM20-17 at 500°C and 1 GPa, to 100°C–300°C at 0.5–2.0 GPa. This had no significant effect on the fluid composition. We then calculated the products of reaction between this fluid and average Samail harzburgite (Table S2 in Supporting Information S1, calculated from Hanghoj et al., 2010) at 100°C–300°C and 0.5–1.0 GPa, at water/rock ratios ranging from 100 to 1.

As a result of data limitations, solid solutions of precipitating minerals were not considered, as the Berman database lacks properties for most Fe-endmembers of minerals commonly observed in listvenites and associated rocks. Thus, for example, the model predicts co-precipitation of pure, endmember magnesite, dolomite and siderite, whereas in listvenite samples we observe Fe-bearing magnesite and dolomite. However, if we add siderite component to magnesite and dolomite, the proportions of the phases closely approximate the observed proportions in drill core. Among the serpentine polytypes, only chrysotile was included in reaction path modeling, since thermodynamic data for antigorite render it too stable at low temperature, while there are no thermodynamic data for lizardite. We did not include goethite. There are no thermodynamic data for a chromian muscovite component, so this was not included, despite the fact that solid solutions ranging from fuchsite to chromian muscovite are observed in MoD Mountain listvenites (e.g., Falk & Kelemen, 2015).

Phase equilibrium calculations constraining the conditions for co-existing graphite (±amorphous carbon compounds) and hematite, and updated calculations for co-existing antigorite and quartz, used (1) Thermocalc (Powell et al., 1998), (2) Perple_X (https://www.perplex.ethz.ch/; Connolly, 1990, 2005, 2009), with the Holland and Powell thermodynamic data for minerals (1998, 2003), and the default equations of state for $H_2O$-$CO_2$ fluids (modified versions of Redlich-Kwong), and (3) SUPCRT (Johnson et al., 1992; Zimmer et al., 2016) with thermodynamic data for minerals from Helgeson et al. (Helgeson, 1978, 1985) or Berman (1988, plus graphite from Helgeson et al.) and various equations of state for $H_2O$-$CO_2$ fluids (Shock et al., 1992, 1997) modified from Helgeson et al. (1981). All of these different combinations provided consistent results, with antigorite + quartz stable with respect to talc at temperatures up to 80°C–120°C.

Results of calculations using the Deep Earth Water (DEW) model (Huang & Sverjensky, 2019; Sverjensky et al., 2014) and the extended Helgeson-Kirkham-Flowers (HKF) aqueous equation of state (Shock et al., 1992, 1997) do not predict equilibrium coexistence of antigorite + quartz above 15°C. Since antigorite-quartz intergrowths in the samples of Falk and Kelemen (2015) indicate coeval crystallization of both phases,

in rocks that formed at >80°C, we presume that these latter results stem from incorrect extrapolation of thermodynamic data to low temperature, and they are not discussed in Section 5.3, below.

### 3.4. (U,Th)/He Ratio Measurements and Cooling Age Calculation

All (U-Th)/He analyses were completed at the UTChron facility at the University of Texas at Austin, using aliquots of zircon separates from the metamorphic sole and lower crustal gabbros, following procedures of Wolfe and Stockli (2010). Individual zircon grains were morphometrically characterized to determine alpha ejection correction (Farley et al., 1996; Cooperdock et al., 2020), equivalent spherical radius (ESR), and estimated mass assuming a tetragonal prism. Single-grain zircon sample aliquots were loaded into Pt tubes for in-vacuo laser He heating for 10 min at ~1200°C by diode laser and $^4$He concentrations were measured by isotope dilution, using a $^3$He tracer, on a Blazers Prisma QMS-200 quadrupole mass spectrometer, after cryogenic purification. Blanks and $^4$He gas standards were run between unknowns to monitor and quantify the procedural baseline during analytical runs. Aliquot laser reheating was repeated (2–5×) until $^4$He gas yields dropped <1% total extracted gas.

After degassing, individual zircon grains were removed from the Pt packets and dissolved using a two-step HF-HNO3 and HCl pressure vessel dissolution technique and measured on a Thermo Element2 HR-ICP-MS following the procedure outlined in Wolfe and Stockli (2010). U-Th-Sm concentrations were calculated using isotope dilution with an isotopically enriched, mixed U-Th-Sm spike calibrated against a 1 ppb U-Th-Sm gravimetric standard solution and blank-corrected using the average of multiple procedural blanks.

Final (U-Th)/He ages were calculated using blank corrected U, Th, Sm and He measurements for each aliquot. Reported concentrations were determined using the morphometrically determined mass of each aliquot. The reported error for individual (U-Th)/He ages represents standard error (8%) based on long-term intra-laboratory reproducibility of Fish Canyon tuff zircon standard, following the approach of Farley (2002). The reported mean sample ages reflect the arithmetic mean of the aliquot ages and their standard deviations.

### 3.5. Calibration of XRF Core Scanner Data

XRF core scanner data were collected onboard DV Chikyu, as described in Kelemen, Matter, et al. (2020). We used the core scanner to analyze nine listvenite samples from BT1B core, and 14 gabbro samples from Hole GT1A core that had known bulk compositions based on XRF analysis at the University of St. Andrews. While onboard DV Chikyu, we used the St. Andrews data to calibrate the XRF data, as follows: wt% $SiO_2$ = 0.89 × (scanner wt% $SiO_2$); wt% MgO = 2.57 + 1.18 × (scanner wt% MgO); wt% $FeO^T$ = 1.048 + (scanner wt% $FeO^T$)0.848; and wt% CaO = 0.878 × (scanner wt% CaO), where $FeO^T$ indicates all Fe is treated as FeO. Fits are illustrated in Figure S2 in Supporting Information S1. Okazaki et al. (2021) present a comprehensive analysis of the XRF scanner data, together with X-Ray tomography data for BT1B core.

### 3.6. Calculation of Mineral Volume Proportions

Volume proportions of quartz, magnesite and dolomite were estimated from bulk rock compositions and XRF scanner data as follows. Weight fractions of $SiO_2$, MgO, $FeO^T$ and CaO were converted to moles in 100 g of rock using their molecular weights. (For all data reported in this paper, the sum of wt% $SiO_2$, MgO, $FeO^T$ and CaO was greater than 90% of the volatile free, bulk rock composition.) The number of moles of dolomite were taken to be equal to moles of CaO, moles of magnesite were calculated as moles MgO—moles CaO, and moles of quartz were taken to be equal to moles of $SiO_2$. All Fe was inferred to be in Fe-oxides and hydroxides. If the small amounts of Fe in carbonate minerals were included in such a calculation, this would slightly increase the proportions of magnesite and dolomite, relative to quartz. Volumes of each mineral in 100 g of rock were calculated using their molar volumes. The data were "projected" from Fe oxy-hydroxides by normalizing the volumes of quartz, magnesite and dolomite to 100%.

## 4. Results

### 4.1. Drilling Operations

Site BT1 is on the north side of the broad channel of Wadi Mansah, which drains mountainous regions to the east and southeast. Hole BT1A penetrated 1.90 m of gravels in Wadi Mansah, south of listvenite outcrops flanking the Wadi. After we became concerned that a steep hole there might intersect tens of meters of gravel before reaching bedrock, and/or that the gravel might overlie a major, steep fault along Wadi Mansah that postdates ophiolite emplacement, we moved the drill and inclined the Hole. Hole BT1B is three or four m closer to the listvenite outcrop. The well head is intact, marked and protected from floods by a concrete monument. Drilling of the fine-grained, silica-rich listvenites was challenging, because this lithology has a hardness similar to fine-grained chert or flint (~7 on the Mohs' scale), but with patience and expert drilling, we obtained ~100% recovery of all lithologies intersected by the borehole. Details of drilling operations are in Kelemen, Matter, et al. (2020).

### 4.2. Mapping and Structural Observations

As noted in Section 2.5, and reported by Falk and Kelemen (2015), MoD Mountain is underlain by a southeast to northwest striking anticline, with its faulted hinge approximately coincident with the ridge along the summit. Exposed contacts between listvenite and serpentinized harzburgite consistently dip to the southwest on the southwest side of the mountain, and to the east and northeast on the northeast side. In the valley north of the mountain, listvenite-harzburgite, listvenite-metamorphic sole, and harzburgite-sole contacts form a broad, shallow syncline. A new, detailed geological map and cross-section, incorporating our lithological and structural observations, is presented in Figure 4.

As shown on the map, in outcrops extending for more than 4 km north of Hole BT1B there is a regular tectonic "stratigraphy", with variably altered peridotite overlying the metamorphic sole, in turn overlying Hawasina Formation sediments, all with low angle fault contacts that have been deformed by a series of gentle, broad open folds evident in the map and cross-section.

We noted normal and reverse shear sense indicators on both sides of the anticline. As a result of the folding, it is difficult to interpret the sense of shear recorded in various outcrops. Some shear sense indicators may predate the folding, while others may record deformation during or after folding.

In contrast, to the northwest and southeast, outside our map area, the outcrop patterns become much more complex, the sole outcrop thins, and there are some vertical fault contacts where all of these older units are juxtaposed with Late Cretaceous Al Khod conglomerates and younger, shallow marine limestones (Stanger, 1985; Villey et al., 1986; Wilde et al., 2002).

### 4.3. Zircon (U,Th)/He Cooling Ages

Zircon (U,Th)/He cooling ages on samples from the metamorphic sole southeast of Fanjah, near MoD Mountain, are $38.7 \pm 7.7$ and $44.4 \pm 8.0$ Ma, cooling ages of zircons from the metamorphic sole at the base of the Wadi Tayin massif to the east are $54.5 \pm 7.4$ and $61.8 \pm 2.6$ Ma, and the cooling age of zircons from the lower crust of the Samail massif is $46.4 \pm 3.9$ Ma (Table S1 and Figure S1 in Supporting Information S1).

### 4.4. Lithology

As illustrated in Figure 5, the top of the Hole sampled ~200 m of listvenite interlayered with two serpentinite bands from 80 to 100 m depth, and 181–185 m depth. Below 185 m, the listvenite is ubiquitously deformed, with visual core descriptions indicating a mixture of brittle and ductile deformation. At about 197 m, core is composed of a few tens of cm of soft, clay-rich fault gouge, together with a few cm of hard, aphanitic, black ultracataclasite. Beneath these fault lithologies, the core sampled ~102 m of the metamorphic sole, grading from dominantly fine-grained, finely-banded, muscovite-bearing metasediments at the top ("greenschists" in Figure 5) to coarser, more massive-appearing, foliated "greenstones", interpreted as metavolcanic rocks, at the bottom.

Serpentinite bands in the core have gradational contacts with host listvenites over 10's of centimeters to ~1 m thick. Serpentinites contain antiaxial veins of magnesite with a median line composed of hematite and other
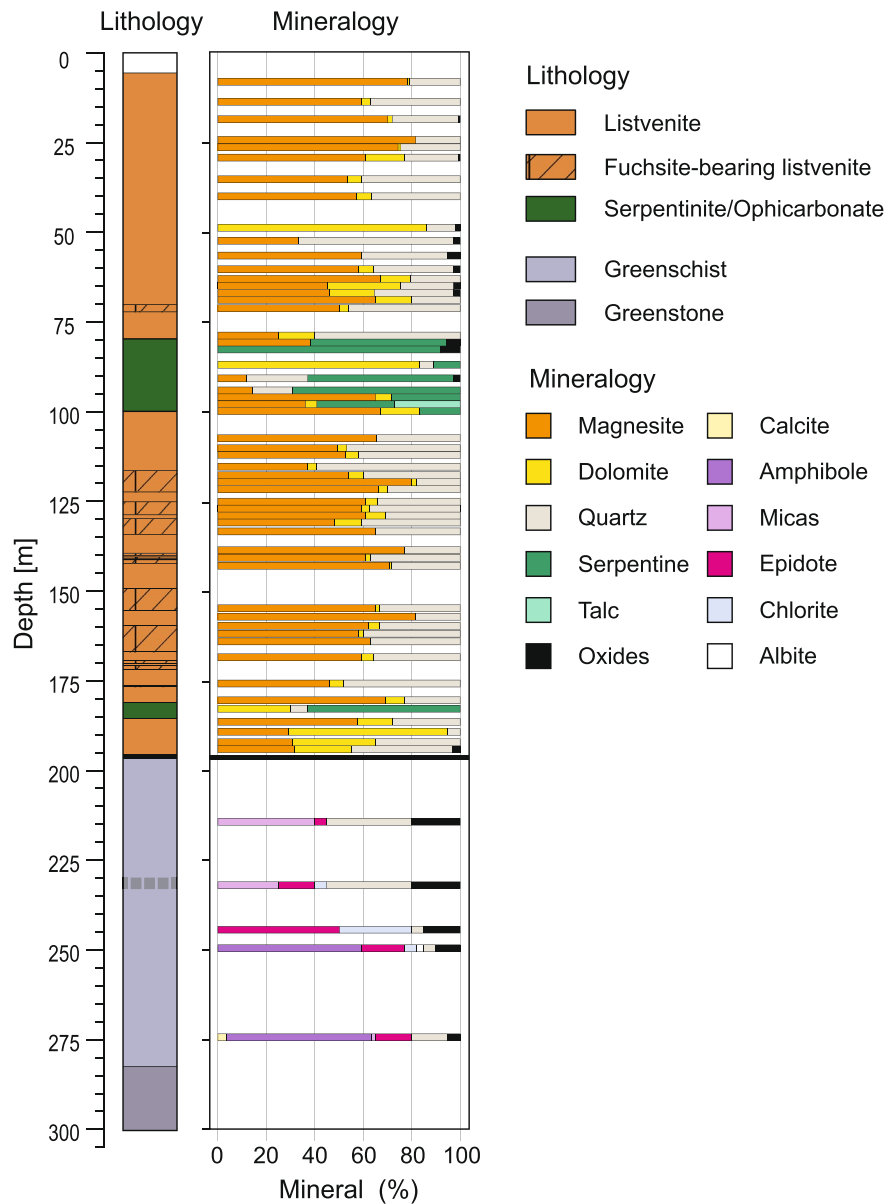
**Figure 5.** Lithologic and mineralogical column for core from Hole BT1B, modified from Godard et al. (2021).

Fe-oxides. There are prismatic terminations of magnesite crystals away from vein centers, toward the host serpentine (Figure 6). Antitaxial veins record growth of minerals outward from the vein center. They are commonly interpreted to open due to the "pressure of crystallization" (Durney & Ramsay, 1973; Urai et al., 1991). However, this interpretation is less clear in the serpentinites and listvenites of Hole BT1B, where the Mg in the carbonate is derived from the host rocks. To some degree these veins may replace, rather than displace, the host.

Between the veins, serpentinites in the core also contain up to 10% magnesite ovoids 10 to 100 microns in diameter, unevenly dispersed within a massive serpentine matrix. These magnesite vein and ovoid textures are abundant in the listvenites as well. Thus, the Shipboard Scientific Party suggested that they are indicative of incipient replacement of serpentinite by listvenite, grading from <10% carbonate (and no quartz) in veins and ovoids to 100% fine-grained carbonate + quartz across sharp reaction fronts (Kelemen, Matter, et al., 2020). Another notable feature is that some of the serpentinites are optically isotropic in thin section, probably indicative of low temperature formation of poorly ordered or amorphous material with serpentine stoichometry (e.g., Andreani et al., 2004).
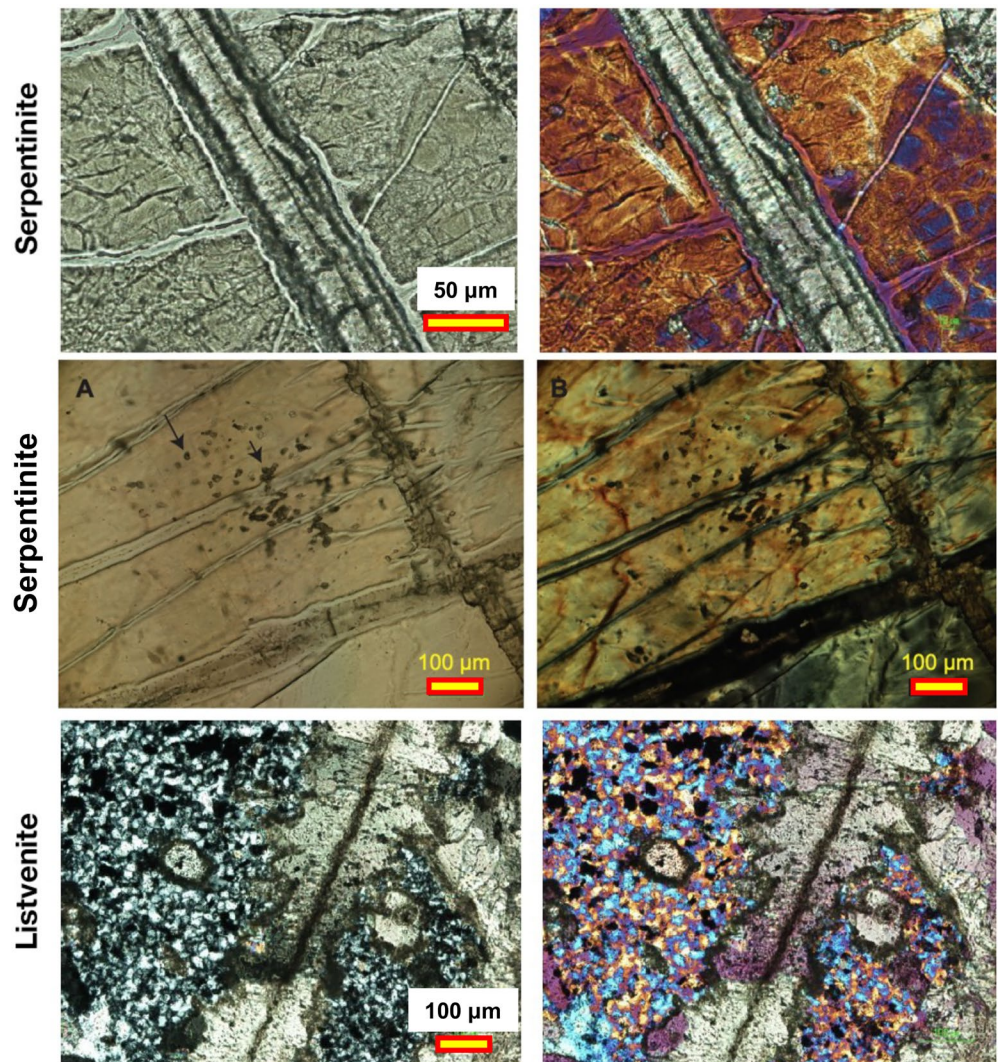
**Figure 6.** Antitaxial magnesite-hematite veins, and magnesite spheroids in serpentinites and listvenites in core from Hole BT1B. Top panels: plane light (left) and crossed-polarized images (right, quartz plate (+1λ) inserted) of magnesite-hematite veins near the lower contact of the upper serpentinite band, TS_BT1B_44Z-3_9-11.5, ~100 m depth, from Figure F47 in Kelemen, Matter, et al. (2020). Middle panels: tiny magnesite spheroids in serpentinite, TS_BT1B_44Z-3_9-11.5, ~100 m depth, from Figure F29 in Kelemen, Matter, et al. (2020). Bottom panels: Cross-polarized images, right one with quartz plate (+1λ) inserted, of texturally similar, "antitaxial" magnesite-hematite veins and magnesite ovoids in quartz-rich, listvenite matrix, TS_BT1B_47Z-3_15-19 at about 110 m depth, from Figure F35 in Kelemen, Matter, et al. (2020).

In turn, listvenites and serpentinites recovered in drill core are hosted by more typical, partially serpentinized peridotites and dunites in outcrop north and northeast of Hole BT1B (Figure 7). Such lithologies, typical of the Banded Unit at the base of the mantle section of the Samail ophiolite, are abundant on the flanks of MoD Mountain, and are particularly well exposed west of the summit (Figure 2) and on the broad, north facing outcrop below the summit ridge.

A sample transect on the ridge forming the drainage divide between Wadi Mansah (site of Hole BT1B) and the parallel wadi north of MoD Mountain documented a 5-m scale progression from listvenite to serpentinite (with intergrown quartz and antigorite) to partially serpentinized peridotite containing relict olivine and orthopyroxene (Figure 5 in Falk & Kelemen, 2015). Along that watershed transect, the presence of antigorite—rather than the serpentine polytypes lizardite and chrysotile—was attributed to high $SiO_2$-activity produced by reaction of olivine and serpentine to produce carbonate and quartz, since antigorite is more $SiO_2$-rich than the other polytypes.
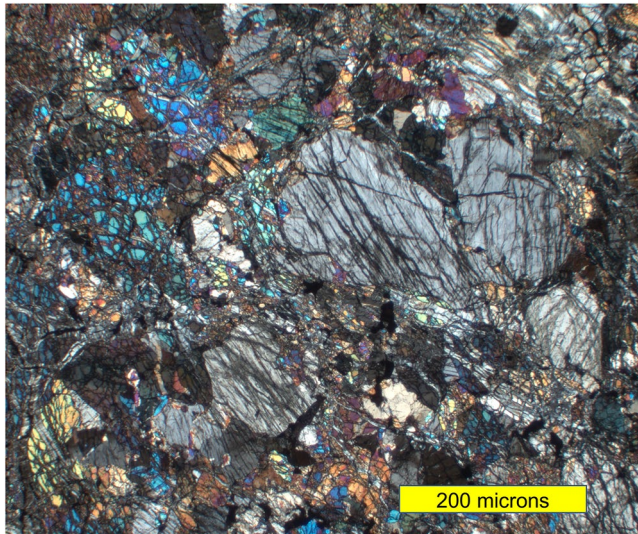
**Figure 7.** Cross-polarized image of partially-serpentinized harzburgite sample OM09-14 (Falk & Kelemen, 2015) from ~10 m above lower listvenite band in Figure 2. Olivine: bright interference colors and irregular, serpentine-filled fractures. Orthopyroxene: gray interference colors and parallel to orthogonal fractures. Minor calcic-pyroxene and/or hornblende are barely visible in this image.

However, the serpentinites in core from Hole BT1B are distinct from the serpentinized zone flanking listvenite on the ridge transect, and from the surrounding, partially serpentinized Banded Horizon harzburgites. Although quartz veins cut the serpentinite in the core, antigorite was not observed. Moreover, despite the presence of some orthopyroxene pseudomorphs ("bastites") in serpentinites, and a concerted effort to find relict mantle minerals, no olivine or pyroxene were detected in drill core. Taken together, field and core observations suggest that the contact between serpentinites and partially serpentinized peridotites is gradational over a few meters at most, approximately as sharp as the contact between listvenites and serpentinites. This is discussed further in Sections 5.7 and 5.8.

Essentially, two types of listvenite were recovered, magnesite + quartz + iron oxide lithologies, and volumetrically less abundant, dolomite + quartz + iron oxide rocks, previously termed magnesite-listvenites and dolomite-listvenites (Falk & Kelemen, 2015). Much of the core contains 0.5%–3% relict chromian spinel, partially or fully altered to Fe-oxides. Instead or in addition, some samples contain minor amounts of Cr-rich white mica (fuchsite-muscovite solid solutions, supplementary Figure 7 in Falk & Kelemen, 2015), in mm to cm scale, ovoid, microscopic intergrowths with quartz. These intergrowths are macroscopically evident in outcrop and core as cm-scale green spots, though in fact Cr-rich mica composes only a few percent of such spots, apparently has undergone alteration to clays in some samples, and was significantly damaged or removed during thin section preparation. As a result, fuchsite crystals recovered from BT1B core are not large enough for $^{40}Ar/^{39}Ar$ analyses. Figure 5 of Nasir et al. (2007) is a photomicrograph of crystalline fuchsite from another listvenite in Oman.

Macroscopic listvenite textures are characterized by abundant veins (10–200 veins more than 1 mm thick per meter of core, typically ~1 per cm) in a fine-grained matrix. In massive listvenites, the fine-grained matrix surrounding veins commonly contains ovoids of magnesite or quartz (Figure 8). Though they have similar textures, ovoids of the two different minerals are rarely adjacent to each other. Both commonly have Fe-oxides in their cores and/or in spherical zones. Microprobe analyses show that some magnesite ovoids have low Fe cores, commonly rimmed with relatively Fe-rich magnesite (Beinlich et al., 2020; Lafay et al., 2020). In other cases, the opposite sense of Fe-zoning is observed (Menzel et al., 2021). All the ovoids have sizes and shapes similar to the quartz spherulites.

Carbonate ovoids and cross-cutting magnesite-hematite veins are also observed in serpentinite bands in the core (Figure 6). Thus, the Shipboard Science Party considered it likely that many such veins initially formed within serpentinite, followed by formation of ovoids within surrounding serpentine, and then by replacement of the entire serpentinite matrix by carbonate + quartz (Kelemen, Matter, et al., 2020). If so, in contrast to conventional interpretations of veins as relatively young features, "cross-cutting" their matrices, in this case the fine-grained listvenite matrix may postdate the earliest veins found within the matrix. This hypothesis is discussed further in Section 5.9

The quartz ovoids have the texture of "spherulites", with radiating microscopic crystals producing a false, "uniaxial interference pattern" in cross-polarized light. Spherulites form during devitrification of amorphous opal as well as rhyolite glass, so Falk and Kelemen (2015) and the Shipboard Science Party (Kelemen, Matter, et al., 2020) interpreted these as replacing opal, which would have been among the earliest $SiO_2$ minerals to form in many of the listvenites. Importantly, opal is commonly found in other listvenites and serpentine-magnesite associations worldwide (Abu-Jaber & Kimberley, 1992; Aftabi & Zarrinkoub, 2013; Akbulut et al., 2006; Arisi Rota et al., 1971; Barnes et al., 1973; Beinlich et al., 2010, Borojević Šoštarić et al., 2014; Boschi et al., 2009; Ece Öi et al., 2005; Jurković et al., 2012; Lacinska & Styles, 2013; Lapham, 1961; Oskierski, Bailey, et al., 2013; Oskierski, Dlugogorski, et al., 2013; Posukhova et al., 2013; Quesnel et al., 2016; Searston, 1998; Ulrich et al., 2014; Zarrinkoub et al., 2005).
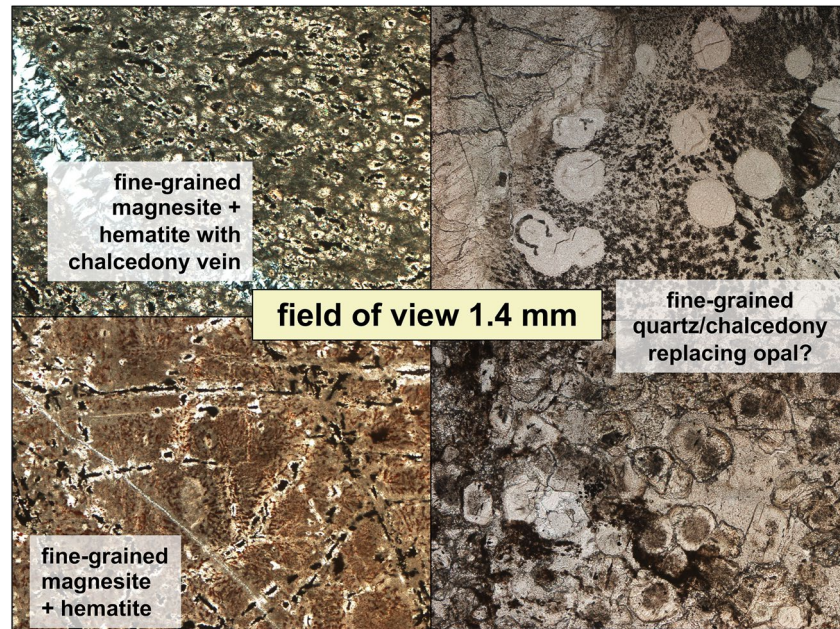
**Figure 8.** Plane light photomicrographs illustrating magnesite ovoids in a matrix composed of magnesite, quartz, and subordinate hematite and Fe-oxyhydroxides, TS_BT1B_20Z-1_42-46, ~40 m depth (left top) and TS_BT1B_27Z-2_6-8.5, ~59 m depth (left bottom), and quartz spherulites with carbonate and hematite inclusions, in matrix of fine-grained quartz and hematite with subordinate, microscopic carbonates, TS_BT1B_60Z-1_12-17, ~140 m depth (right).

Vein types cutting this fine-grained matrix generally record a progression from texturally early, antitaxial magnesite veins—some with cores of hematite + other Fe-oxides (Figure 6)—and related, early Fe-oxide veins, to syntaxial dolomite veins and carbonate-quartz veins, and lastly to syntaxial calcite veins. Some of the late, syntaxial veins contain vugs lined with prismatic calcite and/or dolomite. Syntaxial vein textures record inward crystallization of crystals into fractures that opened due to external, tensional stresses (Durney & Ramsay, 1973; Urai et al., 1991).

A poorly exposed, weathered, fuchsite vein has been observed in outcrop 200 m north of Site BT1B, but no such veins were sampled in BT1B core. We mention this simply to emphasize that Cr and Al were mobile at some stage during listvenite formation or later alteration.

Among the Fe-oxide veins, some contain minor sulfide—generally not detected during core description—and amorphous, organic carbon compounds. The carbon compounds were first identified in core at the drill site, in the lowest listvenite band, as elongate lenses within transposed hematite veins parallel to the penetrative foliation, where they were described as "graphite". Soft organic carbon compounds in these features appear to have been largely lost from sample surfaces during washing and handling of the core prior to shipboard observations and analyses, and again during fabrication of thin sections. However, Raman spectroscopy of small, armored relicts, in oxide veins and also in isolated, dark red spots that resemble relict spinel on the core face and rock slabs, reveals the presence of disordered, thermally immature carbonaceous material (Figure 9), some of which may retain a more ordered organic molecular structure. The carbonaceous materials we can still find, on freshly cut surfaces from the core interior, are commonly on the margins of microscopic chalcocite and covellite crystals, in one case also associated with copper sulphate (chalcanthite)

### 4.5. Crystallographic Preferred Orientation of Minerals

An overall preferred orientation of veins is not evident from structural data on the core scale, possibly due to differential rotation of core pieces. And, systematic measurements have not been made on the outcrop scale. However, at the meter scale many core intervals contain textures indicative of ductile deformation (Figure 10). Some samples show a strong macroscopic foliation, defined by parallel (possibly transposed) veins enclosing
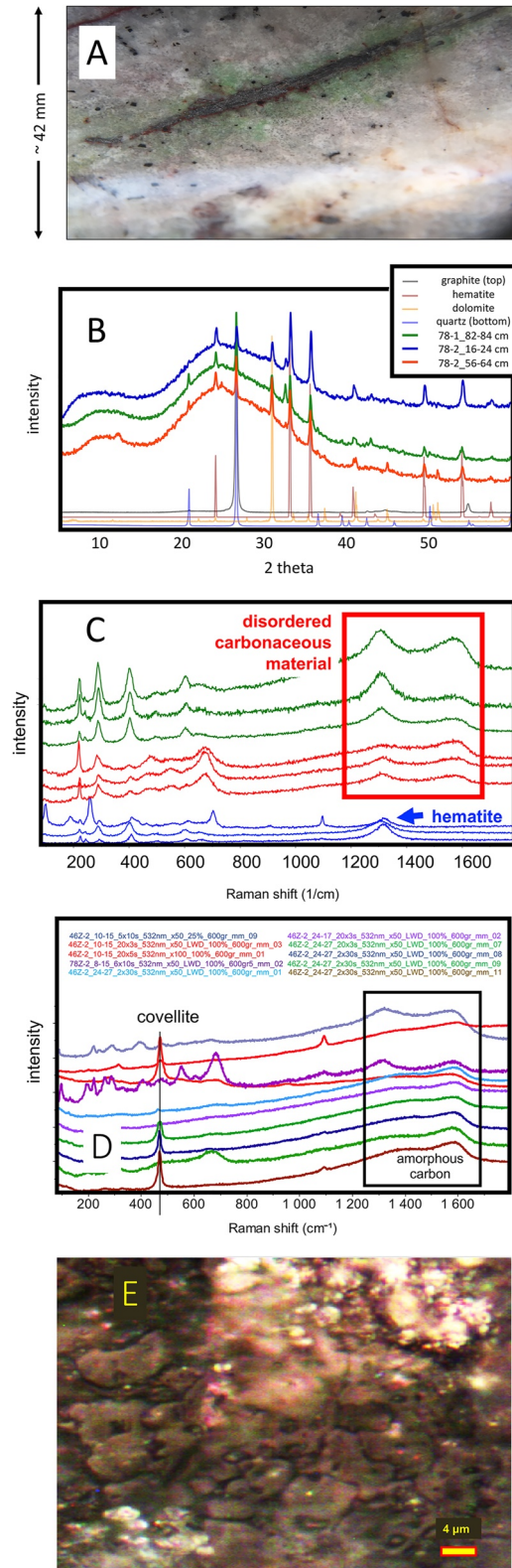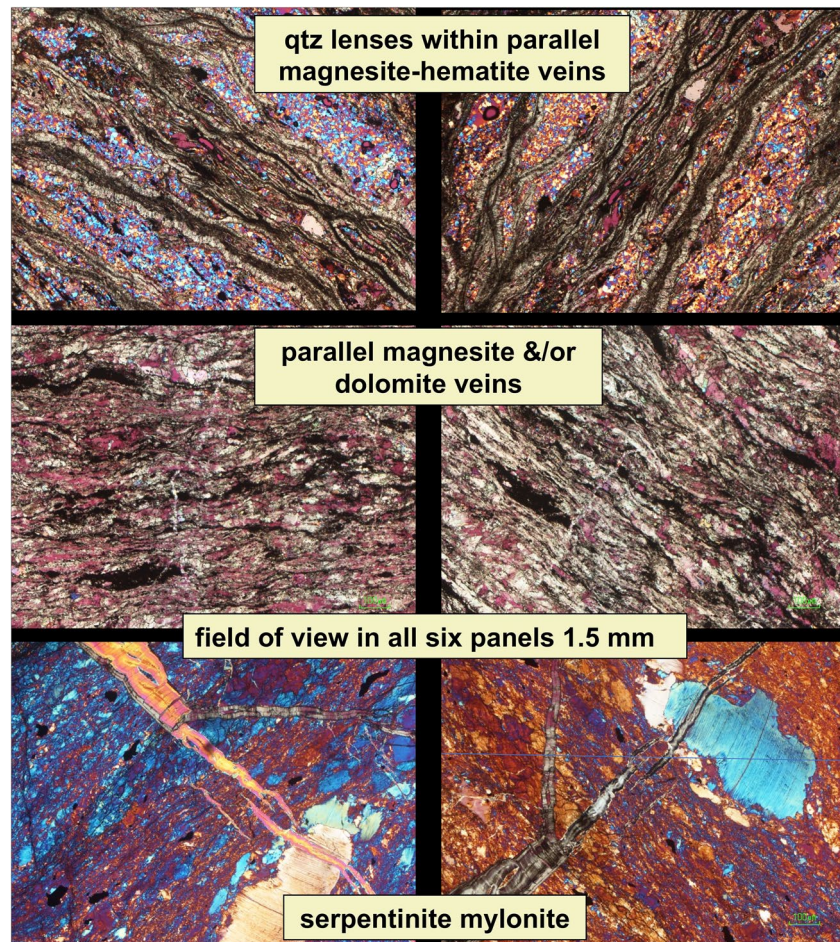
**Figure 9.**

**Figure 10.** Examples of crystallographic preferred orientation (CPO) in localized zones in core from Hole BT1B. All images in cross-polarized light with quartz plate inserted. Images on right are of the same area as on left, but rotated 90° with respect to the polarizers. Areas showing optical continuity have a crystallographic preferred orientation. Top, TS_ BT1B_31Z-4_12-14, ~65 m depth, quartz lenses within sub-parallel, anastomosing magnesite-hematite veins. Middle, TS_ BT1B_78Z-2_34-38, ~195 m, thin section composed almost entirely of parallel magnesite and/or dolomite veins, with a CPO in the carbonates. Bottom, TS_BT1B_74Z-1_59-62, ~183 m, serpentinite mylonite, with a strong CPO in the fine-grained matrix, and visible, internal deformation in serpentine porphyroclasts.

elongate lenses of the fine-grained matrix, in textures commonly interpreted to form via boudinage during ductile deformation. In samples with a strong foliation defined by dozens of subparallel, early magnesite veins per 10 mm2, intervening patches of fine-grained quartz commonly have a crystallographic preferred orientation (CPO). Some samples with a strong foliation defined by abundant, subparallel (tectonically transposed?) carbonate veins also have an optically evident, crystallographic preferred orientation in magnesite and/or dolomite. Similarly,

**Figure 9.** Carbonaceous material in drill core. (a) Drill site photo of 1–2 mm vein of shiny, gray, soft material described as graphite on the drill site, in a vein rimmed with hematite. Field of view 5 cm wide, core 74Z-01, ~195 m depth. (b) Shipboard XRD spectra of soft "graphite" powder extracted from veins with "graphite" + hematite, replacing Figure F43 in Kelemen, Matter, et al. (2020). Interpretation of these data is complicated by the similarity of the quartz and graphite peaks at ~26° 2Θ, but quartz also has a prominent peak at ~21°C which is absent from the blue spectrum for 78Z-02_16-24. (c) Raman spectra of black material in samples BT1B_77Z-03_30-38 (blue), 78Z-02_8-15 (red) and 78Z-02_50-56 (green, ~192–198 m depth. Broad double peaks at wavenumbers of ~1350/cm and 1600/ cm are indicative of disordered carbon compounds; no Raman spectra diagnostic of graphite were obtained. Many microscopic, soft, black domains contained hematite, with a single broad peak at ~1350/cm, instead of, or in addition to, disordered carbon compounds. (d) Raman spectra of black material in samples BT1_44Z-02_10-15, BT1_78Z-02_8-15, and BT1_44Z-02_24-27, showing broad, double peaks indicative of disordered carbon compounds, some associated with covellite. Core 44Z ~98 m depth. (e) dark gray copper sulphate "cow pies", spatially associated with brightly reflecting covellite, near amorphous carbon material, field of view ~100 microns, sample BT1_44Z-02_24-27. Data and images from core 44Z are from a 1 mm diameter black spot with a red rim in the interior of the core, exposed by the rock saw during sample preparation.

some shear zones in serpentinite have an optically evident, strong shape- and crystallographic-preferred orientation of lizardite crystals, and contain deformed serpentine porphyroclasts.

### 4.6. Brittle Deformation Textures

A broad range of different breccias and cataclasites are observed in listvenites and in the metamorphic sole, in outcrop and in core. In turn these are cut by sharp faults—some associated with planar bands and branching veins of aphanitic ultracataclasite and/or pseudotachylite—and by late calcite veins. The nature and interpretation of cataclasites and faults observed in core from Hole BT1B are discussed in detail by Menzel et al. (2020).

### 4.7. Geochemical Data

The bulk composition of core samples was measured in five different ways: (1) Major and minor element compositions of nine samples were measured by XRF at St. Andrews University. (2) Major and minor element compositions of 74 samples, including those previously analyzed at St. Andrews, were measured via XRF (both fusion and pressed pellets) onboard the Drilling Vessel Chikyu. (3) Major element compositions of the cut face of selected core sections were analyzed onboard using an XRF core scanner. (4) Trace element compositions of a few samples were analyzed onboard via ICP-MS. (5) Trace element compositions of 61 samples were analyzed via ICP-MS at the Université de Montpellier. These data, and subsequent analyses, are tabulated and described in Kelemen, Matter, et al. (2020) and Godard et al. (2021), so for brevity we simply refer readers to those other publications.

## 5. Discussion

### 5.1. Subduction Zone Setting of Listvenite Formation

On the basis of their structural observations west and northwest of the MoD Mountain area, and U/Pb formation or cooling ages from cross-cutting calcite veins ($60 \pm 16$ and $58 \pm 6$ Ma) Scharf et al. (2020) infer that listvenites in the Fanjah area postdate ophiolite emplacement, echoing the qualitative ideas of Stanger (1985) and Wilde et al. (2002). As noted in Sections 2.5 and 4.2, our geochronological and field observations are inconsistent with this interpretation. The listvenite mineral isochron age of $97 \pm 29$ Ma ($2\sigma$; Falk & Kelemen, 2015) yields a 93% chance ($1.5\sigma$) that the listvenites formed before 75 Ma, while subduction beneath the ophiolite was still active, and a 97% chance that the listvenites formed before 68 Ma. Thus, the isochron data support listvenite formation during subduction, and show that the calcite veins cutting listvenite, dated by Scharf et al., are ~10 million years younger than listvenite formation.

In this paper, our mapping and structural observations indicate an intact tectonic "stratigraphy" around the basal thrust of the ophiolite, encompassing the allocthanous Hawasina metasediments, overlain by the metamorphic sole, in turn overlain by Banded Unit dunites and harzburgites of the Samail ophiolite mantle section, with essentially horizontal lithologic contacts extending for kilometers. This is the stratigraphy created during subduction beneath the ophiolite, and—together with the isochron—it indicates that these units were juxtaposed during low angle thrusting along the subduction zone. In turn, all the listvenites in the MoD Mountain area are less than a kilometer away from the basal thrust, and have contacts with surrounding mantle peridotites and the metamorphic sole that are parallel to the basal thrust. All these data, taken together, indicate that the listvenites formed along and above the basal thrust of the ophiolite during subduction.

### 5.2. Faulting, Deformation and Veining After Listvenite Formation

(U,Th)/He cooling ages (Section 4.3) indicate that the region around MoD Mountain cooled very slowly, remaining above the closure temperature for He diffusion in zircon, ~180°C (Reiners et al., 2004), or were reheated above this temperature, during 30–60 million years after formation of the igneous crust in the ophiolite and peak metamorphism of the sole. Based on textural observations, it is clear that the breccias and cataclasites sampled in BT1B drill core postdate listvenite formation (Menzel et al., 2020). Some may postdate ophiolite emplacement, and may be broadly related to Paleocene to Miocene uplift and extension during formation of the nearby Jebel Akdar and Saih Hatat domes. On the other hand, some could be related to deformation during subduction beneath
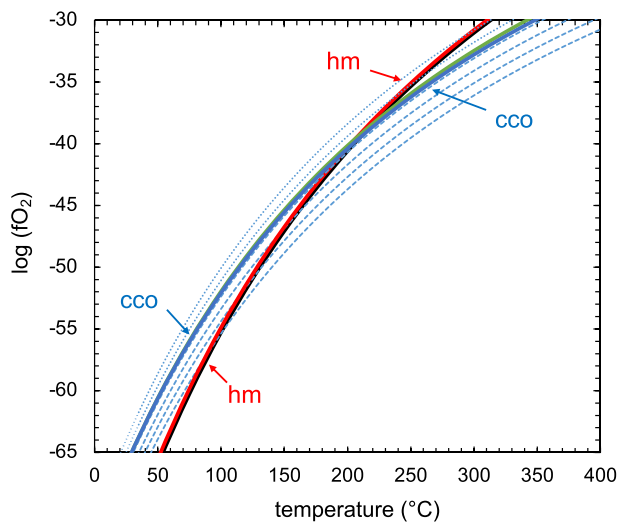
**Figure 11.** Diagram illustrating temperature and oxygen fugacity for the well-known oxygen buffers, hematite-magnetite (hm, $6Fe_2O_3 = 4Fe_3O_4 + O_2$) and graphite-carbon dioxide (cco, $C + O_2 = CO_2$). Graphite and amorphous carbon compounds are stable below the cco curves, while hematite is stable above the hm curve. hm curves are solid red (1 GPa) and black (0.2 GPa). cc curves are solid green (1 GPa) and blue (0.2 GPa). Dashed blue curves are for cco at 0.2 GPa total pressure, with $P(CO_2) = 0.1$, 0.01, 0.001 and 0.0001 GPa from left to right. Dotted blue curves are for cco at 0.2 GPa total pressure = $P(CO_2)$, with a reduced activity of graphite (i.e., amorphous carbon compounds) 0.01 and 0.1 from left to right.

the ophiolite. The long term persistence of temperatures above 180°C in this region renders it difficult to distinguish formation from cooling ages using (U,Th)/He data.

### 5.3. Temperature of Listvenite Formation

The temperatures of listvenite formation have been previously constrained using metamorphic phase equilibria, conventional oxygen isotope thermometry, and clumped isotope analyses. Falk and Kelemen (2015) noted the presence of intergrown antigorite (serpentine) + quartz in the reaction zone between listvenite and serpentinite on the west ridge of MoD Mountain (Figure 2). In some cases, these samples also contain talc. They used Thermocalc (Powell et al., 1998), with thermodynamic data from Holland and Powell (1998, 2003), and similar methods using the thermodynamic data of Gottschalk (1996), to estimate that equilibrium coexistence of antigorite, quartz and talc occurs at 80°C–120°C, depending on the choice and uncertainty of thermodynamic parameters for the minerals, and the (poorly known) pressure at which these assemblages crystallized. For this paper, we obtained similar results using Perple_X (Connolly, 1990, 2005, 2009).

The temperature estimates based on co-existing antigorite + quartz are broadly consistent with temperature estimates based on $\delta^{18}O$ in quartz and carbonate minerals in the listvenite, assuming that fluid $\delta^{18}O$ was similar to seawater, and with clumped isotope analyses of magnesite and dolomite yielding temperatures of 80°C–130°C for listvenite samples (Falk & Kelemen, 2015). Observation of quartz spherulites in listvenite, possibly reflecting devitrification of opal, also suggests that listvenite formation occurred at "low temperature", ~150°C or less, in the presence of aqueous fluid.

Here we show that veins of intergrown amorphous carbon compounds and hematite sampled in the core also must have formed below ~200°C (Figure 11). The observation of "reduced" hydrocarbon species intergrown with oxidized iron minerals in veins may seem surprising at first, but they are mutually stable at low temperature due to the stronger temperature dependence of the iron oxidation state, compared to the carbon oxidation state. Above ~200°C, reduced, organic carbon compounds and oxidized iron minerals such as hematite cannot coexist at the same oxygen fugacity, but they can crystallize together at moderate oxygen fugacities below ~200°C. We've found that this result is robust across all available sets of internally consistent thermodynamic data, and in the pressure range from 0.2 to 1.0 GPa.

As an aside, we note that in products of experimental reaction between carbon-bearing fluids and olivine at 185°C, hydrostatic pressure of 25 MPa, and $P(CO_2)$ of 1 MPa, Peuble et al. (2019) observed formation of hematite and organic carbon compounds (their Figure 8), but calculated that these phases were not in equilibrium together at these low $CO_2$ partial pressures (their Figure 11). In general, high P/T subduction zone conditions render formation of organic carbon compounds relatively likely during fluid/rock reaction in the mantle wedge, while these compounds are comparatively unlikely to form in lower pressure alteration and weathering environments.

Returning to the topic of listvenite formation temperatures, 14 more recent clumped isotope analyses for listvenites and carbonate-bearing serpentinites from BT1B core yield an average temperature of 147 ± 58°C (1σ). 10 of the 14 temperature estimates lie within the 1σ range, whereas two are lower (45 ± 5 and 52 ± 8°C) and the two least precise estimates are higher (227 ± 52 and 247 ± 52°C; Beinlich et al., 2020). Though a few MoD Mtn listvenites might have formed at temperatures greater than 200°C, such temperatures are too high for crystallization of intergrown amorphous carbon + hematite, they are too high for crystallization of intergrown antigorite + quartz, and they are too high for crystallization of opal. Also, carbonation of peridotite above ~150°C would form abundant talc + magnesite, whereas talc is absent in most MoD Mountain listvenites, and rare in serpentinite-listvenite contact zones that are gradational over a few meters (Falk & Kelemen, 2015; Kelemen, Matter, et al., 2020).

The range in temperature estimates based on phase equilibrium and clumped isotope ratios from the MoD Mountain listvenites may indicate that mineral assemblages in the listvenites and surrounding serpentinites formed gradually over a range of times and temperatures. In addition, some of the clumped isotope data may record closure temperatures during cooling, rather than the peak temperature at which the MoD Mountain listvenites first crystallized, as proposed for clumped isotope data from fine-grained 10-m scale magnesite veins in California (Garcia del Real et al., 2016). Alternatively, since the highest clumped isotope temperatures from Beinlich et al. are also the most imprecise estimates, perhaps they result from analytical uncertainties or disequilibrium effects. When the 14 clumped isotope temperatures from Beinlich et al. are combined with the 31 older clumped isotope temperatures from Falk and Kelemen, the full data set yields an average of $100 \pm 46°C$ ($1\sigma$), with the highest temperatures from Beinlich et al. falling outside the $2.5\sigma$ (99% probability) range.

### 5.4. Depth of Listvenite Formation

The depth of listvenite formation is difficult to constrain. As noted in Section 2.4, published work on the metamorphic sole beneath the Samail ophiolite reports peak temperatures up to 700°C–900°C at pressures ranging from 200 to 1400 MPa, indicative of anomalously hot subduction zone conditions. Common peak pressure estimates, ~1200 MPa, indicate depths exceeding the structural thickness of the ophiolite. Thus, either (1) the published range of pressure estimates for the metamorphic sole is the result of uncertainty rather than true variation in depth, and/or (2) the lower few km of the ophiolite mantle section has undergone thinning in some places, and/or (3) the lenses of the metamorphic sole recording the highest pressures migrated upward with respect to the overlying peridotite, and/or (4) some mineral equilibria record tectonic overpressures rather than lithostatic loads. Also, we infer from Sr isotope data that the fluids that formed the listvenites were not derived from the metamorphic sole (Section 5.6, below, and de Obeso, Kelemen, et al., 2022). For all these reasons, it is unclear whether the metamorphic pressures inferred for the sole constrain the depth of listvenite formation. However, temperatures and pressures recorded by the sole do provide a window into the thermal evolution of subduction beneath the ophiolite before and during listvenite formation.

Initiation of subduction, during formation of the metamorphic sole, involved thrusting of a hot mantle wedge over newly formed, hot basaltic crust. Over time, subduction of progressively older oceanic crust and—eventually—the pelagic sediments of the Hawasina Formation would have caused cooling of the subduction zone as it evolved toward a steady state geotherm. A few clumped isotope analyses on calcite in sediments beneath the ophiolite and the metamorphic sole on MoD Mountain yield temperatures of 150°C–200°C (Falk & Kelemen, 2015). It is possible that these were peak temperatures during diagenesis of the sediments along a late, steady state subduction geotherm at the pressure and depth recorded by the metamorphic sole in core from Hole BT1B, 800–1200 MPa, or about 25–40 km.

In turn, even lower temperatures for most listvenite samples may record continued, isobaric cooling of rocks flanking the subduction zone. Temperatures of 100°C–200°C at depths of 25–40 km are inferred for fore-arc regions above subduction zones from heat flow data (reviewed in Peacock, 1996) predicted for steady state, oceanic subduction geotherms in numerical models (e.g., Peacock, 1996; Peacock et al., 2005; Syracuse et al., 2010), including those recently modeled by van Keken et al. (2019), and lie within the cold end of the range of PT conditions recorded by subduction-related metamorphic rocks (Hacker, 1996, 2006; Penniston-Dorland et al., 2015). Such low temperatures at 25–40 km are rare or absent in other tectonic environments.

To summarize, it is possible that the sediments and the overlying mantle peridotites at the base of the ophiolite were juxtaposed by subduction at the leading edge of the mantle wedge, at a depth of 25–40 km, and that the MoD Mountain listvenites formed at these depths along a cold, steady state subduction geotherm. Alternatively, if the metamorphic sole has migrated updip with respect to the overlying peridotites, then the listvenites could have formed at lower pressures and shallower depths.

### 5.5. Composition of Listvenite Protolith and Geochemical Fluid Additions

Given the abundance and variety of mineralogically simple veins, many of which are monomineralic, there is substantial compositional variation in listvenites at the millimeter to meter scale. This variability extends to larger scales in some parts of the core. Nevertheless, remarkably enough, average $MgO/SiO_2/FeO*$ (all Fe as FeO) ratios in the listvenites are very similar to those in average residual peridotites from the ophiolite (Figure 12), as
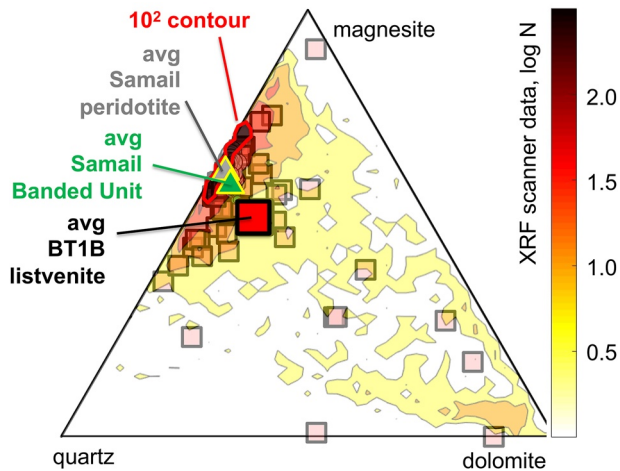
**Figure 12.** Ternary diagram illustrating volume proportions of quartz, magnesite and dolomite, projected from hematite, calculated from whole rock compositions, for Samail mantle peridotites (average in gray triangle, data as large, gray open circles, barely visible beneath the averages and the 102 contour area, Godard et al., 2000; Hanghoj et al., 2010; Monnier et al., 2006), Banded Unit peridotites near the base of the Samail ophiolite mantle section (small, green open circles, barely visible, Falk & Kelemen, 2015; Khedr et al., 2013, 2014; Takazawa et al., 2003), and listvenites from Hole BT1B and MoD Mtn (open squares, Falk & Kelemen, 2015; Kelemen, Matter, et al., 2020), superimposed on contoured histogram of mineral proportions from shipboard XRF scanner data. Contour interval 10½. Okazaki et al. (2021) provide more thorough interpretation of shipboard XRF scanner data plus X-Ray Computed Tomography data on the whole core. Average listvenite, Banded Unit and Samail mantle peridotite compositions are provided in Table S2 in Supporting Information S1.
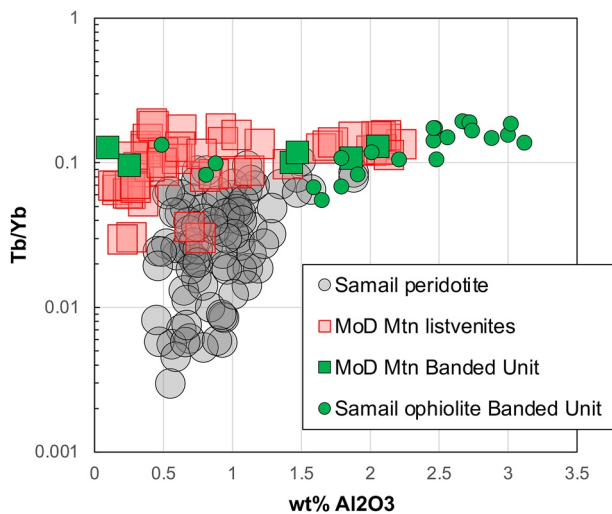


**Figure 13.** Wt% $Al_2O_3$ versus Tb/Yb ratios in bulk rock compositions of MoD Mtn listvenites (open squares, Falk & Kelemen, 2015; Godard et al., 2021; Kelemen, Matter, et al., 2020), and MoD Mountain peridotites that host listvenites (green squares, Falk & Kelemen, 2015; Godard et al., 2021), compared to typical Samail mantle peridotites (gray open circles, Godard et al., 2000; Hanghoj et al., 2010; Monnier et al., 2006), and Banded Unit peridotites from the base of the ophiolite (Khedr et al., 2013, 2014; Takazawa et al., 2003).

discussed further by Okazaki et al. (2021). These oxides comprise more than 90% of the volatile-free bulk composition of the rock. These data suggest that there was little dissolution and export of major elements from the rocks during transformation of peridotite to serpentinite and then to listvenite as discussed further in Section 5.9.

On the other hand, serpentinites and listvenites record addition of tens of weight percent $H_2O$ and $CO_2$ to the original bulk composition of mantle peridotite protoliths. In addition to $CO_2$, dolomite listvenites clearly record substantial addition of CaO, and—since CaO and Sr concentrations are strongly correlated—of Sr as well.

Although the shipboard data do not reveal systematic variation in the abundance of magnesite versus dolomite listvenites downhole, there is a clear change in the abundance of both Al and K, together with many other highly incompatible trace elements. Concentrations of these elements are relatively low above the serpentinite band at 80–100 m depth, and much higher below that band (Godard et al., 2021; Kelemen, Matter, et al., 2020).

Understanding the source for enrichment in these elements is complicated by uncertainty about their concentration in the peridotite protolith. As noted in Sections 2.3, 2.5 and 4.4, a "Banded Unit" of alternating dunite, harzburgite and lherzolite characterizes the base of the ophiolite mantle section in many regions. Some Banded Unit peridotites record high temperature geochemical "refertilization" by reaction of residual mantle peridotites with infiltrating melt or fluid at >800°C, with addition of calcic pyroxene and Mg-rich hornblende. This produced enrichment in CaO and $Al_2O_3$ to levels well above those in typical residual mantle peridotites in the Samail ophiolite (Godard et al., 2000; Hanghoj et al., 2010; Monnier et al., 2006). Indeed, four out of six harzburgite samples from the Banded Unit on MoD Mountain have Ca and Al contents outside the 1σ range of variability in residual mantle peridotite in the ophiolite (Falk & Kelemen, 2015; Godard et al., 2021; Kelemen, Matter, et al., 2020).

The listvenites below 100 m depth in core from Hole BT1B have trace element ratios that are distinct from typical peridotites, but characteristic of the Banded Unit (Figure 12 and Godard et al., 2021), as shown in Figure 13. In particular, middle to heavy rare earth element ratios in the Banded Unit, and in the listvenites, are high compared to typical Samail peridotites. Such enrichment in middle rare earth elements is commonly associated with the presence of igneous hornblende in peridotites. Thus, the listvenites probably inherited these characteristics from the enriched, Banded Unit protolith.

On the other hand, it is clear that most listvenites have higher Sr concentrations than typical Samail ophiolite peridotites and the Banded Unit (de Obeso, Kelemen, et al., 2022). This observation suggests that both Sr and Ca were added during low temperature alteration, along with $H_2O$ and $CO_2$. These topics are discussed further by Godard et al. (2021).

## 5.6. Source of Fluid for Listvenite Formation

Present day Sr isotope ratios in listvenites and serpentinites from MoD Mtn range from ~0.708 to 0.715 (de Obeso, Kelemen, et al., 2022; Falk & Kelemen, 2015). Using current Rb/Sr contents in these samples, age corrected 87Sr/86Sr ratios at 96 Ma range from ~0.708 to 0.714, much higher than the range of Sr ratios in Samail ophiolite peridotites (0.703–0.707, Benoit et al., 1999; Gerbert-Gaillard, 2002; Gregory & Taylor, 1981; Lanphere

et al., 1981; McCulloch et al., 1980, 1981), the range in Late Cretaceous to modern seawater (~0.7075 to 0.7081), or the range in peridotite-hosted ground water in the Samail ophiolite (~0.7065 to 0.7092, Weyhenmeyer, 2000). Thus, the Sr-, Ca- and $CO_2$-rich fluid(s) that modified the mantle overlying the basal thrust of the ophiolite had relatively high 87Sr/86Sr ratios compared to fresh, residual mantle peridotites.

Initially, we expected that the metamorphic sole, as sampled by core from Hole BT1B, might be the source of fluids that formed listvenites in overlying peridotites, or at least might be analogous to the source of these fluids. However, this is not consistent with the Sr isotope data on the sole in core from Hole BT1B. Measured and age-corrected Sr isotope ratios in the metamorphic sole are consistently lower than corresponding ratios in the listvenites (de Obeso, Kelemen, et al., 2022).

Instead, pelagic, clastic units of the underlying Hawasina sedimentary rocks have measured and age-corrected Sr isotope ratios that span the same range as those in the listvenites (de Obeso, Kelemen, et al., 2022). Thus, these sedimentary units in the Hawasina may be analogous to subducted sedimentary rocks that produced $CO_2$-bearing fluids which, in turn, formed the MoD Mountain listvenites. This is likely, despite the presence of C- and Sr-rich limestone and dolomite units with lower Sr isotope ratios in the Hawasina Formation, because devolatilization of clay and mica bearing, clastic metasediments produces abundant, $CO_2$-rich aqueous fluids, while limestone and marble remain relatively refractory at low to moderate temperature, subduction zone conditions (e.g., Kerrick & Connolly, 2001; Stewart & Ague, 2020).

Indeed, there is evidence for a deeply subducted component with terrigenous isotope characteristics—like those of the Hawasina clastic sedimentary rocks—elsewhere in the Samail ophiolite. A series of felsic intrusions in the sole, mantle and lower crust along the length of the ophiolite have low, age-corrected $^{143}Nd/^{144}Nd$ (and thus, presumably, high $^{87}Sr/^{86}Sr(t)$), attributed to melting of high-grade metasediment in the subduction zone below the ophiolite (Amri et al., 2007; Briqueu et al., 1991; Cox et al., 1999; Haase et al., 2015, 2016; Lippard et al., 1986; Rioux, Benoit, et al., 2021; Rioux, Garber, et al., 2021; Rioux et al., 2013; Rollinson, 2015; Spencer et al., 2017).

A complication is that the clastic units in the Hawasina formation have $\delta^{13}C$ less than −4 per mil, whereas listvenites have $\delta^{13}C > -3$ per mil. These differences in carbon isotope ratios can be understood as the result of temperature dependent carbon isotope fractionation. As discussed in more detail in de Obeso, Kelemen, et al. (2022), at temperatures greater than ~300°C, dissolved $CO_2$ in aqueous fluids has $\delta^{13}C$ higher than co-existing calcite and dolomite (Deines, 2002; Horita, 2014). At lower temperatures, calcite and dolomite have $\delta^{13}C$ higher than co-existing fluids. Dolomite and magnesite crystallized at relatively low temperature, from aqueous fluids that acquired their carbon isotope ratios during higher temperature devolatilization of Hawasina clastic sediment compositions, would have $\delta^{13}C$ in the range of 1.0 to −3.0‰, as observed in the MoD Mountain listvenites. In addition, low carbon solubilities in low temperature, low pressure aqueous fluids saturated in carbonate minerals in mineral assemblages similar to those in the Hawasina clastic sedimentary rocks (Figure 22 and associated text in Chapter 4, Falk, 2014; Kelemen & Manning, 2015) may be insufficient to produce the MoD Mountain listvenites (de Obeso, Kelemen, et al., 2022; Falk & Kelemen, 2015).

Based on the data and reasoning described in the previous paragraph, we hypothesize that subduction zone devolatilization at 400°C–700°C produced $CO_2$-rich aqueous fluids that then cooled and decompressed by flow up the subduction zone, and reacted with peridotite at less than 200°C to produce the MoD Mountain listvenites. To quantify this hypothesis, we made thermodynamic calculations with the compositions of solid reactants given in Table S2 in Supporting Information S1, methods described in Section 3, and results outlined in Figure 14 and 15. As the source of fluid, we chose sample OM20-17, a pelitic end-member from among the Hawasina clastic sedimentary rocks analyzed by Falk and Kelemen (2015) and de Obeso, Kelemen, et al. (2022). As the peridotite reactant, we used an average Samail harzburgite composition calculated from published studies (Godard et al., 2000; Hanghoj et al., 2010; Monnier et al., 2006).

Devolatilization of clastic Hawasina sediments, such as OM20-17, is predicted to produce fluids with ~20,000 ppm dissolved C at ~400°C to ~700°C along subduction zone geotherms (Figure 14). Closed system decompression and cooling of fluid produced from OM20-17 to 100 to 300°C, and 0.5–1 GPa produced no significant change in the composition of this modeled fluid (Modeling open system, reactive transport of this fluid, updip along a subduction zone geotherm, is beyond the scope of this paper, as is modeling the fate of subduction zone fluids that have more than 10 wt% $CO_2$—predicted for mixed siliciclastic-carbonate rocks (Figure 14)—as they cool and decompress).
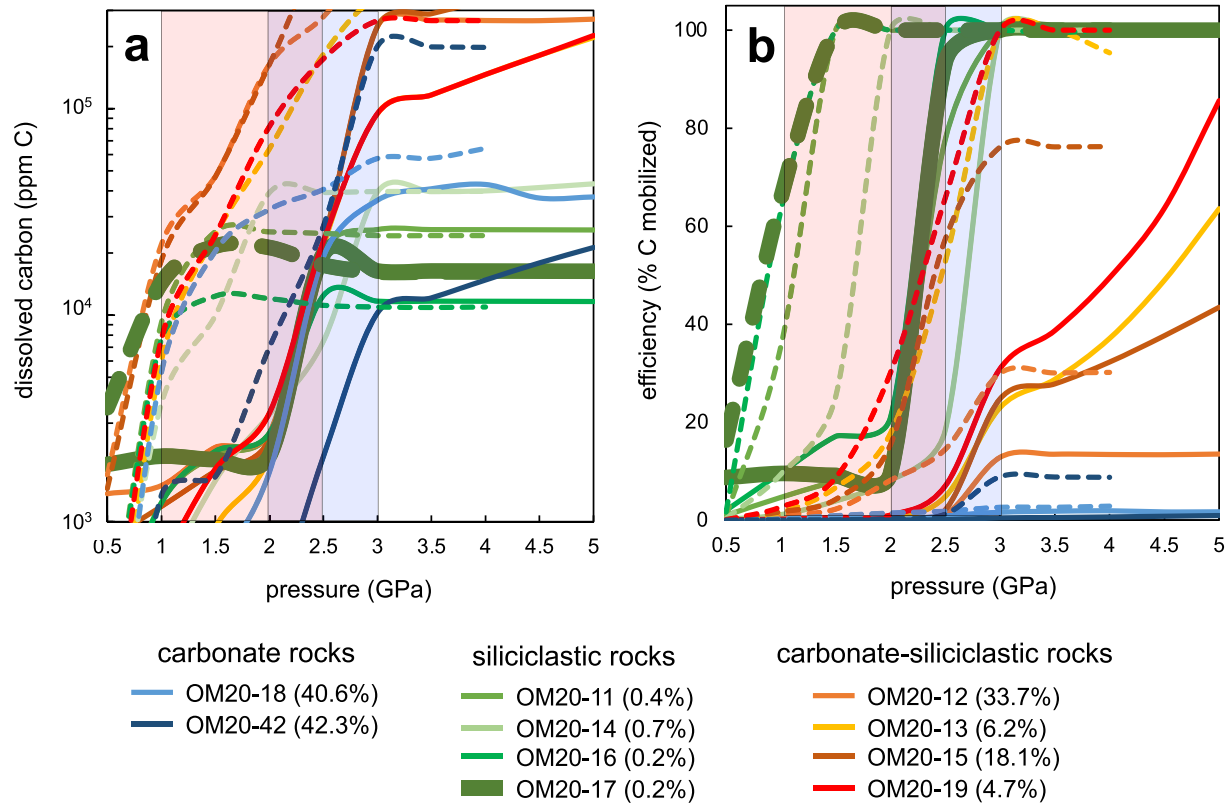
**Figure 14.** Dissolved carbon concentrations (a) and extent of carbon removal (b) in calculated fluids equilibrated with the compositions of Hawasina sediments in the MoD Mountain area (Supplementary Table 1 in de Obeso, Kelemen, et al., 2022), at a water/rock ratio of 5%, evolving along cold and hot subduction geotherms. Solid curves are calculated along the cold geotherm (Chile, Marianas) and dashed curves along the hot geotherm (Mexico, Cascades) from Syracuse et al. (2010). Blue and red rectangles outline the pressure range for subduction zone temperatures of 400°C–700°C along cold and hot geotherms, respectively. The initial carbon contents of the rocks (wt%, all carbon as $CO_2$) are given in the legend. Siliciclastic rocks are predicted to lose all of their carbon between 400 and 700°C, forming fluids with 1–3 wt% dissolved carbon. Mixed carbonate-siliciclastic lithologies are predicted to lose varying proportions of their total carbon in this temperature range, and form fluids with >10 wt% C, Carbonate rocks retain most of their carbon, but also form fluids with a few weight percent carbon in this pressure and temperature range. From among these results, a fluid in equilibrium with OM20-17 (bold green lines) at 500°C and 1 GPa, cooled to 100°C–300°C at 0.5–2 GPa, was used to model reaction of carbon-bearing subduction zone fluids with Samail ophiolite peridotite (Section 5.7). Fluid and peridotite reactant compositions are given in Table S2 in Supporting Information S1.

## 5.7. Listvenite Formation

Reaction of the model fluid from OM20-17 with peridotite at 100°C–300°C and 0.5–1.0 GPa is predicted to produce mineral assemblages similar to those modeled by F. Klein and Garrido (2011): (1) Small masses of "birbirite" (silicified peridotite) at high water/rock ratios and/or low temperatures, through (2) moderate masses of listvenite and soapstone (talc-carbonate rocks) at moderate water/rock and temperature, to (3) relatively large masses of carbonate-bearing serpentinite at low water/rock ratios and/or high temperature (Figure 15). Predicted magnesite and quartz proportions correspond closely to observed proportions in MoD Mtn listvenites (Figure 12). Most of the PT conditions we modeled produced small amounts of hematite coexisting with magnesite and quartz, as observed. Predicted magnesite and siderite proportions correspond to a solid solution with ~8 wt% FeO, which is a few wt% higher than observed in MoD Mtn listvenites. Most modeled conditions produced dolomite in listvenite assemblages at water/rock ratios less than 10 (log water/rock = 1), consistent with the presence of relatively late, cross-cutting dolomite-bearing veins in the listvenites. Most model runs produce small amounts of kaolinite, and very limited proportions of muscovite, in listvenite mineral assemblages, consistent with the widespread presence of minor amounts of chromian white mica in MoD Mtn listvenites, and in listvenites worldwide. It is possible that addition of a thermodynamic model for fuchsite would yield larger proportions of white mica, and correspondingly smaller proportions of kaolinite, over a wider range of temperature and water/rock ratios. Also, perhaps some of the green sheet silicates in listvenites are chrome-bearing clays rather than micas.
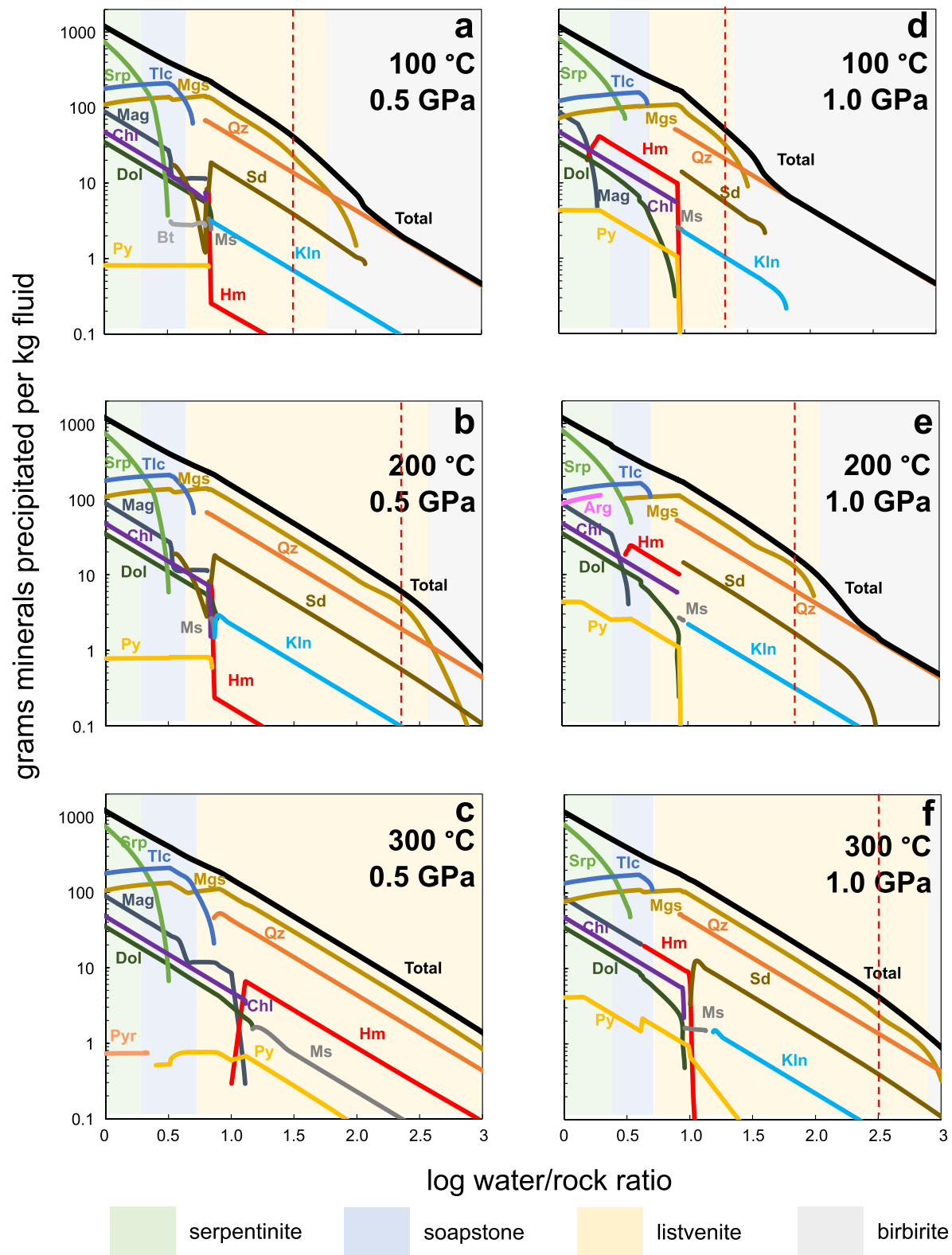
**Figure 15.** Results of thermodynamic reaction path models of reaction between fluids derived from devolatilization of Hawasina pelitic sedimentary rock sample OM20-17 (Section 5.6) and average Oman harzburgite. Mineral end-member abbreviations Qz quartz, Sd siderite, Mgs magnesite, Kln kaolinite, Ms muscovite, Dol dolomite, Chl chlorite, Py pyrite, Tlc talc, Srp serpentine (chrysotile), Pyr pyrrhotite. Red, vertical dashed line indicates where magnesite/quartz molar and volume proportions are ~2:1, as observed in magnesite listvenites from MoD Mtn (e.g., Figure 12).

Thus, thermodynamic modeling suggests that the $CO_2$-bearing aqueous fluids that formed the MoD Mountain listvenites formed by metamorphic devolatilization in a subduction zone at >400°C. Some of these fluids then migrated updip to react with peridotite at the leading edge of the mantle wedge, probably at a depth less than 40 km, while others probably reacted with the mantle at greater depth.

Subhorizontal lenses of listvenite at MoD Mountain contain a cumulative mass of about 2 billion tons of $CO_2$ over a strike length of 2 km NS, and 5 km EW, corresponding to 1 million to 400,000 tons of $CO_2$ per m along strike. The allochthonous sedimentary units below the ophiolite are about 3 km thick. Within these, clastic units comprise at least half the section, and contain about 2300 ppm C, or 0.84 wt% $CO_2$ on average (de Obeso, Kelemen, et al., 2022), yielding a total of about 35 tons $CO_2$ per m along strike, per m subducted. (As noted above, rocks composed mainly of calcite and/or dolomite in the subducting sedimentary section would be unlikely to contribute significant amounts of $CO_2$ to subduction fluids at temperatures less than 800°C.) At subduction velocities of 0.05–0.1 m/year, 90% decarbonation of the clastic units in the Hawasina Formations with a density of 2.75 tons/m3, at ~400°C to 500°C would produce at least 1.7–3.5 tons of $CO_2$ per year per m of strike length. If most of this $CO_2$ reacted with peridotite at the depth and temperature of MoD Mtn listvenite formation, this could supply the observed mass of $CO_2$ at MoD Mountain in less than 600,000 years.

Most of the model results at different conditions predict precipitation of a few weight percent magnesite (and some dolomite) in the serpentinization domain. This is consistent with observation of carbonate veins in serpentinites from Hole BT1B, and with the hypothesis that formation of carbonate veins in the serpentinite zone preceded transformation of the serpentinite host rocks to listvenite (also see Figure 6 and associated text in Section 4.4), The fluid temperatures, compositions and fluxes used in these calculations are different from the constraints used in some calculations by Falk and Kelemen (2015). In that previous work, we explored the possibility that $CO_2$ to form the listvenites was supplied over tens of millions of years, carried in 100°C–200°C fluids containing a few hundred ppm dissolved carbon, derived from pore fluids and/or dewatering of opal and clay minerals, from the Hawasina sedimentary rocks immediately below the site of listvenite formation at MoD Mountain. However, one of us (Falk!) insisted on mentioning the possibility that the $CO_2$ to form listvenites was derived from fluids formed deeper in the subduction zone, that migrated updip. We now prefer this latter hypothesis, for the reasons outlined above.

Updip migration of fluids in a subduction zone has been predicted in some simplified dynamic models of fluid flow in a viscously deforming subduction zone with high permeability (Wilson et al., 2014). However, the tendency of fluid buoyancy to drive vertical fluid flow may often dominate subduction zone fluid fluxes. Thus, formation of relatively shallow listvenites, like those at MoD Mountain, may be localized and unusual. Elsewhere, $CO_2$-bearing fluids may migrate vertically into overlying mantle peridotite at greater depth (e.g., Kelemen & Manning, 2015). It is interesting to ponder how subduction zone $CO_2$ fluxes may be partitioned between these different transport and mineralization processes.

## 5.8. Multiple Reaction Fronts

The thermodynamic models presented in Sections 5.6 and 5.7 provide a starting point for understanding "chromatographic effects" during transformation of peridotite to serpentinite. As can be seen in Figure 15, our reaction path models predict sharp fronts where serpentinite is replaced by soapstone, and then by listvenite. Talc-bearing, soapstone assemblages are predicted to crystallize in a limited range of conditions, consistent with the fact that talc is rare in core from Hole BT1B, and in hand specimens from MoD Mtn, where it is almost entirely restricted to narrow (~1 m scale) transition zones between listvenite and serpentinite. If we were to use different thermodynamic data, talc might be even less abundant, or absent in models at 100°C, because talc is predicted to be unstable below ~100°C with respect to antigorite + quartz when using mineral data from Holland and Powell or Gottschalk, together with the Redlich-Kwong equation of state for $H_2O$-$CO_2$ fluids as modified by Kerrick and Jacobs (1981) and by Holland and Powell (2003).

In the model results presented in Figure 15, with reaction progress increasing from high fluid/rock ratios on the right to low fluid/rock ratios on the left, magnesite + quartz and magnesite + talc become unstable with respect to serpentine as dissolved carbon in the fluid is exhausted. Because carbon is a minor constituent of aqueous fluid, but a major component of the listvenite assemblage, exhaustion of dissolved carbon is predicted to occur at

a fluid/rock ratio much greater than 1 (log fluid/rock >0). Of course, because aqueous fluid is composed mainly of $H_2O$, the potential for serpentinization of peridotite continues to much lower fluid/rock ratios.

Although we cannot model it, we can also predict that—in the presence of pervasive fluid flow on the grain scale—there could also be a sharp front where serpentine replaces olivine at water/rock ratios less than one. Thermodynamic calculations for simplified olivine serpentinization by Kelemen, Evans, et al. (2020) indicate that olivine + $H_2O$ would be stable with respect to serpentine at 100°C and a partial pressure of $\sim 10^{-2}$ bars, and at 200°C and $P(H_2O) \sim 1$ bar. While these conditions cannot be modeled using EQ3/6, we can anticipate that low partial pressures of $H_2O$—much lower than lithostatic pressures—are produced along grain boundaries and near the tips of incipient fractures and veins, especially where fluid has been almost completely consumed by peridotite hydration reactions. Under these conditions, there could be a sharp front where serpentine (at higher fluid pressures) becomes stable relative to olivine (at lower fluid pressure).

Throughout the mantle section of the Samail ophiolite, residual mantle peridotites commonly contain about 50%–80% serpentine, as inferred from the fact that bulk rock analyses yield loss on ignition (mostly, $H_2O$) of 8–10 wt% as compared to 13–16 wt% $H_2O$ in completely serpentinized, Mg end-member harzburgite and dunites. These partially serpentinized peridotites commonly show a "mesh texture", with relict olivine and pyroxene "cores" transected by a "mesh" of cross-cutting serpentine veins—typically 10 to 100 microns apart (Francis, 1956; Green, 1961, 1964; Raleigh & Paterson, 1965). In some regions within the Samail ophiolite, particularly areas of relatively subdued topography that have undergone extensive, penetrative weathering, relict mantle minerals in the mesh cores are completely replaced by serpentine (e.g., OmanDP Sites BA1, BA2, BA3 and BA4, Kelemen, Matter, et al., 2020; Kelemen et al., 2021). However, along the steep canyons and narrow ridges that are typical of outcrops in the mantle section of the ophiolite, subject to relatively rapid erosion, the pervasive presence of the serpentine vein mesh surrounding relict mantle minerals attests to relatively rapid fluid transport in fractures and veins, compared to slow transport of $H_2O$ into the mesh cores by diffusion and/or imbibition.

In contrast, as noted above, the serpentinites sampled in core from Hole BT1B contain no relict olivine or orthopyroxene, though pyroxene pseudomorphs ("bastites") are evident. A zone of 100% serpentinized peridotites a few meters thick was sampled by Falk and Kelemen (2015) in a transect across a listvenite-peridotite contact on the watershed ridge east of the summit MoD Mountain. Outside this zone, samples of peridotite had compositions and textures typical of partially serpentinized residual mantle peridotites throughout the ophiolite. Based on these observations, we infer that there is a 100% serpentinite zone a few meters thick, with sharp fronts—less than a meter thick, between serpentinte and listvenite on one side, and between partially and completely serpentinized peridotite on the other side.

### 5.9. Volume Change During Listvenite Formation

The likely volume change during fluid-rock reactions has long been debated. Whereas Coleman and Keith (1971) proposed that serpentinization involved simple addition of $H_2O$ to peridotite, with no significant change in the volatile-free solid composition, Carmichael (1987), Nahon and Merino (1997), and Fletcher and Merino (2001) argued that such reactions take place at nearly constant volume, with addition of some components balanced by dissolution and export of others. Fletcher & Merino provided quantitative calculations to support this hypothesis. Where a fluid that is super-saturated in a new mineral phase, A, starts to crystallize A within a host mineral B that is initially in equilibrium with fluid, expansion of B around A leads to an increase in local effective stress. In turn, because chemical potential is proportional to the mean stress, this reduces supersaturation in A and leads to undersaturation in B. This process continues, with very small volume changes, until the rate of crystallization of A becomes equal to the rate of dissolution of B, at a steady state stress.

Using the methodology of Fletcher and Merino (2001) and a saturation index of 2 (as they did), Kelemen and Hirth (2012) calculated that the steady state, effective stress during replacement of olivine with serpentine is $\sim 40$ MPa. However, because olivine is very far from equilibrium with water at low temperature, the saturation index for water reacting with olivine to form serpentine at 50°C–250°C and $P(H_2O) > 1$ bar is close to $10^7$, and the steady state, effective stress estimated using the method of Fletcher and Merino is $\sim 800$ MPa (Kelemen & Hirth, 2012). Clearly, such a large differential stress cannot be sustained within most rocks, which will deform at a lower stress, before the steady state can be reached, either via ductile mechanisms (if reactions are slow and temperatures are high) or via fracture and frictional deformation (if reactions are fast and temperatures are low).

The latter outcome is sometimes termed "reaction-induced cracking" (Jamtveit et al., 2009; Rudge et al., 2010) or "reaction-driven cracking" (Kelemen & Hirth, 2012). Thus, while some workers still disagree over the extent of volume change in specific replacement processes, the approach of Fletcher and Merino nicely explains a continuum between nearly constant volume replacement of one mineral by another at high temperature, close-to-equilibrium conditions, and large volume changes accommodated by fractures and frictional sliding at low temperature, far-from-equilibrium conditions.
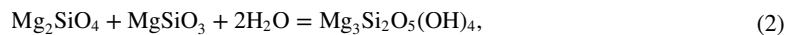
As noted in Section 5.5, despite dramatic, local variability, the average major element composition of listvenites from MoD Mountain—in drill core and surface samples—is strikingly similar to the average composition of residual mantle harzburgites in the Samail ophiolite. The fact that average Mg/Si/Fe ratios in the listvenites are almost identical to those in Samail peridotites suggests that (1) large scale dissolution of the peridotite protoliths was nearly congruent, exporting dissolved, major elements in approximately their initial proportions, or (2) there was little dissolution and export of major elements in the protolith during addition of $CO_2$ to form listvenites, and addition of $H_2O$ to form serpentinites.

Thermodynamic models, experimental data, and observations of natural rock samples strongly favor the second of these hypotheses. The solubility of silicate and Fe-oxide minerals in rock-buffered aqueous fluids at low temperature is too low to allow for large scale dissolution and export of major elements in open system, fluid-rock reactions. In turn, models of addition of $CO_2$ and/or $H_2O$ to peridotites, predict very little removal of other species, together with large increases in the mass and volume of the solid products of reaction. Birbirite formation may involve net volume and mass loss due to extensive dissolution of peridotite reactants at water/rock ratios greater than ~100. However, the models of listvenite formation illustrated in Figure 15 yield predicted mass and volume increases of 10%–55% relative to an anhydrous, peridotite reactant, as illustrated in Figure 16. Similar results have been produced by thermodynamic models of serpentinization (volume increase of 40%–60%, de Obeso & Kelemen, 2018; Malvoisin, 2015), experimental observation of closed system serpentinization (30%–60%, F. Klein & Le Roux, 2020) and analysis of microstructures in partially serpentinized peridotites formed in an open system (59 ± 30% to 74 ± 36%, Malvoisin et al., 2020).
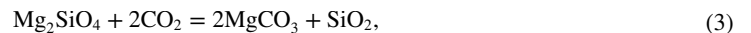
These modeled and observed volume changes approximate those resulting from simplified, Fe-free, stoichiometric reactions. Thus, hydration of olivine to form serpentine and brucite,
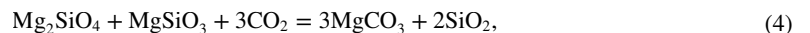
$$2Mg_2SiO_4 + 3H_2O = Mg_3Si_2O_5(OH)_4 + Mg(OH)_2, \tag{1}$$
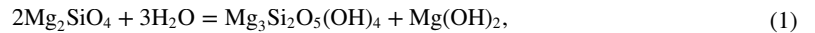
and hydration of olivine + orthopyroxene to form serpentine,

$$Mg_2SiO_4 + MgSiO_3 + 2H_2O = Mg_3Si_2O_5(OH)_4, \tag{2}$$

can produce 52% and 63% increases in the solid volume, respectively. (Volume change calculated as 100% (product volume - reactant volume)/(reactant volume)). Direct carbonation of olivine
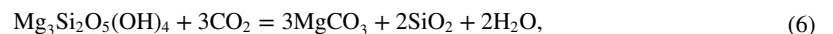
$$Mg_2SiO_4 + 2CO_2 = 2MgCO_3 + SiO_2, \tag{3}$$

and olivine + orthopyroxene,

$$Mg_2SiO_4 + MgSiO_3 + 3CO_2 = 3MgCO_3 + 2SiO_2, \tag{4}$$

can lead to 85% and 74% increases in the solid volume, respectively. And, carbonation of serpentine plus brucite

$$Mg_3Si_2O_5(OH)_4 + Mg(OH)_2 + 4CO_2 = 4MgCO_3 + 2SiO_2 + 3H_2O, \tag{5}$$

and serpentine alone

$$Mg_3Si_2O_5(OH)_4 + 3CO_2 = 3MgCO_3 + 2SiO_2 + 2H_2O, \tag{6}$$

both produce solid volume increases ~22%.

Additional constraints on, and discussion of, the solid volume increases during formation of the MoD Mountain listvenites are provided by Godard et al. (2021).
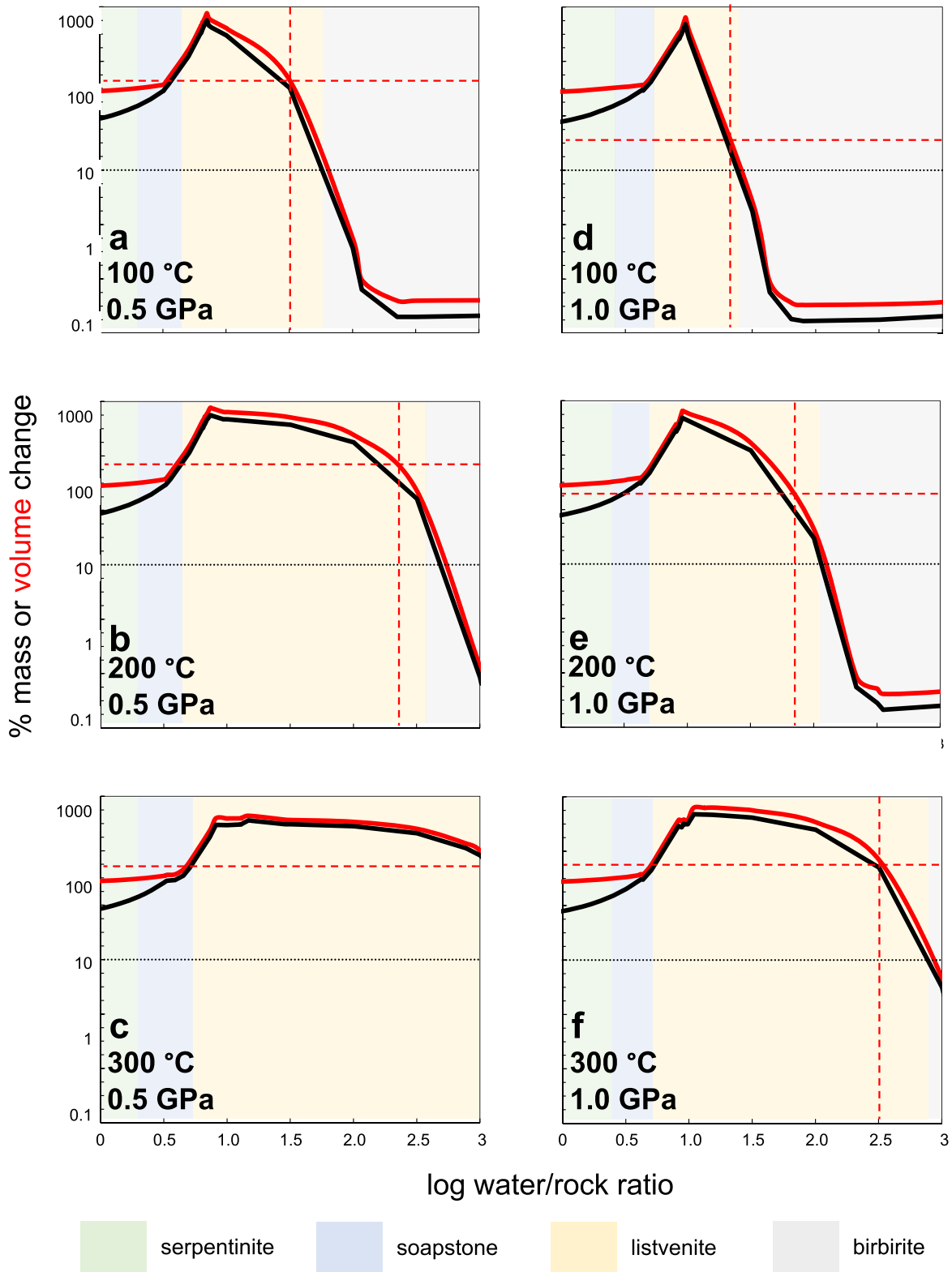
**Figure 16.** Calculated mass and volume change relative to an anhydrous peridotite, for the reaction path models illustrated in Figure 15. Dashed, vertical red lines indicate where molar and volume proportions of magnesite/quartz reach 2:1, as onserved in MoD Mtn listvenites (e.g., Figure 12). Dashed, horizontal line highlights the minimum increase in solid volume calculated for listvenite formation.
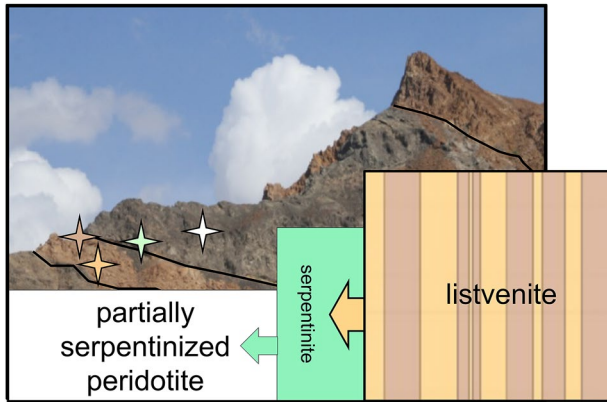
**Figure 17.** Schematic illustration of sequential volume changes during replacement of partially serpentinized peridotite by serpentinites and then replacement of serpentinites by listvenites. The height of the rectangles corresponds to the relative volumes, produced by reaction of $CO_2$-bearing fluid with an initial, anhydrous peridotite. The tan and brown stripes in the "listvenite" represent alternations of different listvenite compositional bands. Stars on photo of the SW side of MoD Mtn illustrate position of listvenite, serpentinite and partially serpentinized peridotite samples (Falk & Kelemen, 2015).

Because porosities in peridotite, serpentinite and listvenite rarely if ever exceed 5%, all of these solid volume changes must be accommodated mainly by expansion of the entire rock volume. It is interesting to speculate how much uplift—and/or lateral expansion—in forearc regions is caused by hydration and carbonation of the mantle wedge. However, at the plate tectonic scale, the rates of reactions similar to those outlined in Equations 1–6 are unknown. It is likely that the strains due to reaction are comparable to, or smaller than, other rates of deformation at convergent plate boundaries, rendering the effect of solid volume expansion difficult to detect at the regional scale.

Based on the considerations outlined in this section, it is likely that large increases in the solid volume occurred during formation of the MoD Mountain listvenites, and were accommodated mainly by reaction-driven cracking, frictional sliding along existing fractures, and/or reaction-assisted granular flow (Menzel et al., 2021). The presence of abundant, antitaxial magnesite, magnesite-hematite, and Fe-oxide veins in both serpentinites and listvenites is qualitatively consistent with a reaction-driven cracking process. However, we have not identified any obvious strain markers that would allow a quantitative evaluation of this hypothesis using rock textures.

Building upon an idea from Hansen et al. (2005), the Shipboard Scientific Party developed the hypothesis that large volume increases due to hydration of olivine and pyroxene (reactions 1 & 2) may have initially formed fractures at (and beyond) a serpentinization front—not observed in drill core, but traversed by Falk and Kelemen (2015)—and these fractures were conduits for fluid flow and sites of localized deformation during the smaller volume changes due to carbonation of serpentinites (reactions 5 and 6) as schematically illustrated in Figure 17.

### 5.10. Low Temperature Ductile Deformation in Subduction Zones

As noted above, the listvenites at MoD Mountain may have formed at depths of 25–40 km, at temperatures less 200°C, yielding low temperature "geotherms" of 5–8°C/km depth. Such small increases of temperature with depth are characteristic of the forearc above subduction zones (Peacock, 1996). High fluid pressures at these depths may account for the somewhat surprising indications of low temperature, ductile deformation in core samples from Hole BT1B, based on the observed crystallographic preferred orientation (CPO) in quartz, magnesite and serpentine in core samples (Section 4.4; Figure 10).

Some of the fabrics illustrated in Figure 10 could be inherited. For example, in early formed, magnesite-hematite veins, magnesite forms parallel crystals, perpendicular to vein margins, with small misorientations between adjacent crystals. When these veins are parallel (because they form that way, or after they are transposed), this imparts a CPO to the sample, and may also give the impression that sub-grain boundaries are present, even if there was no deformation of magnesite crystals via dislocation creep. Similarly, quartz replacing opal may inherit a CPO, or a CPO may arise due to anisotropic stress during recrystallization, without substantial strain.

On the other hand, the serpentine mylonite illustrated in Figure 10 almost certainly records large strains due to distributed deformation along grain boundaries. Moreover, clear examples of ductile deformation and shear zones with classical indicators of substantial strain indicate that ductile deformation was active during the initial stages of listvenite formation, perhaps assisted by positive feedback between weakening, due to reaction-induced recrystallization, and porosity enhancement due to deformation, as discussed by Menzel et al. (2021). An important role for ductile deformation in reaction zones at the top of subducting oceanic crust may help to explain why, in the relatively hot Cascadia and SW Japan subduction zones, there are very few earthquakes at the top of the subducting crust (Abers et al., 2009, 2013; Hirose et al., 2008).

## 6. Conclusions

Observations of drill core of listvenite (completely carbonated peridotite), serpentinite, and subduction-related metamorphic rocks from OmanDP Hole BT1B provide constraints on temperature, depth, and deformation during mass transfer of $H_2O$ and $CO_2$ from subducted sediments into overlying mantle peridotites at the leading edge of the mantle wedge. Listvenites, and a surrounding zone of serpentinite, formed at temperatures less than ~200°C and poorly constrained depths of 25–40 km. Serpentinization and carbonation involved reaction of partially serpentinized, residual mantle peridotite with $CO_2$-rich, aqueous fluids produced by devolatilization of subducting, clastic sediments analogous to the Hawasina formation, probably at 400°C–600°C. These fluids cooled as they were transported up the subduction zone to the site of listvenite formation.

Such processes could play a significant role in the global carbon cycle. Not all listvenites form above subduction zones. However, listvenites are found at and near the basal thrust in other ophiolites, worldwide (Akbulut et al., 2006, Borojević Šoštarić et al., 2014; Escayola et al., 2009; Menzel et al., 2018; Quesnel et al., 2016; Scarsi et al., 2018; Sofiya et al., 2017; Ulrich et al., 2014). The leading edge of the mantle wedge—and subduction modified mantle that has later been incorporated into the continental mantle lithosphere—may be a globally important reservoir for carbon (Foley & Fischer, 2017; Kelemen & Manning, 2015; Li et al., 2017; Scambelluri et al., 2016)

During BT1B listvenite formation, total solid volume increased by tens of percent due to hydration followed by carbonation. While core and surface samples provide few direct constraints on the mechanism that accommodated this expansion, one hypothesis is that large volume changes during hydration of olivine and pyroxene along a serpentinization front caused large stresses and fractures that accommodated expansion via frictional sliding, and provided secondary porosity for the $CO_2$-rich fluids that transformed serpentinites to listvenites.

Based on observed crystallographic preferred orientation in quartz, magnesite and serpentine in macroscopically identified shear zones, it is inferred that ductile deformation of listvenite and serpentinite occurred under low temperature conditions at the base of the mantle wedge during subduction. Low temperature ductile deformation, coeval with serpentinization and listvenite formation, may have been facilitated by recrystallization associated with the hydration and carbon mineralization processes, as discussed in more detail by Menzel et al. (2021). Such a process could be active in subduction zones where the interface between subducting oceanic crust, sediments, and hanging wall peridotites is aseismic.

## APPENDIX A

### Phase 1

### Onsite Drilling Team

Peter Kelemen, Department of Earth and Environmental Sciences, Columbia University, New York, NY, USA, peterk@ldeo.columbia.edu; Jürg M. Matte, Project Director, School of Ocean and Earth Science, University of Southampton, Southampton, UK, J.Matter@southampton.ac.uk; Damon Teagle, School of Ocean and Earth Science, University of Southampton, Southampton, UK, Damon.Teagle@southampton.ac.uk; Jude Coggon, Project Manager, School of Ocean and Earth Science, University of Southampton, Southampton, UK, jude.coggon@southampton.ac.uk; Juan Carlos de Obeso, Department of Earth and Environmental Sciences, Columbia University, New York, NY, USA, deobeso@ldeo.columbia.edu; Michelle Harris, Geography, Earth and Environmental Sciences, Plymouth University, Plymouth, UK, michelle.harris@plymouth.ac.uk; Emma Bennett, School of Earth and Ocean Sciences, Cardiff University, Cardiff, UK, bennette7@cardiff.ac.uk; Nico Bompard, School of Ocean and Earth Science, University of Southampton, Southampton, UK, N.Bompard@soton.ac.uk; Marine Boulanger, Department of Petrology, Center de Recherches Pétrographiques et Géochimiques (CRPG), Vandœuvre-lés-Nancy, France, marineb@crpg.cnrs-nancy.fr; Lyderic France, Department of Geosciences, CRPG-CNRS Université de Lorraine, France, lyde@crpg.cnrs-nancy.fr; Gretchen Früh-Green, Department of Earth Sciences, Federal Institute of Technology, Zurich, Switzerland, frueh-green@erdw.ethz.ch; Dieter Garbe-Schönberg, Institute of Geosciences, Christian-Albrecht University of Kiel, Kiel, Germany, dgs@gpi.uni-kiel.de; Benoit Ildefonse, Department of Géosciences, CNRS Université de Montpellier, Montpellier, France, benoit.ildefonse@umontpellier.fr; Ana Jesus, Department of Applied Geosciences, German University of Technology in Oman, Oman, ana.jesus@gutech.edu.om; Craig Manning, Department of Earth, Planetary and Space Sciences, University of California, Los Angeles, CA, USA, manning@epss.ucla.edu; Dominik Mock, Institute for Mineralogy,

Leibniz University of Hanover, Hanover, Germany, dom.mock@web.de; Tony Morris, Geography, Earth and Environmental Sciences, Plymouth University, Plymouth, UK, amorris@plymouth.ac.uk; Samuel Müller, Institute of Geosciences, Kiel University, Kiel, Germany, mail.sam@gmx.net; Julie Noël, Department of Geosciences, Université de Montpellier, Montpellier, France, Julie.Noel@gm.univ-montp2.fr; Daniel Nothaft, Department of Geological Sciences, University of Colorado, Boulder, CL, USA, daniel.nothaft@colorado.edu; Americus Perez, Department of Earth Sciences, Kanazawa University, Kanazawa, Japan, adperez@stu.kanazawa-u.ac.jp; Philippe Pezard, Department of Geosciences, CNRS Université de Montpellier, Montpellier, France, ppezard@gulliver.fr; Nehal Warsi, Drilling Consultant, School of Ocean and Earth Science, University of Southampton, Southampton, UK, nhwarsi@gmail.com; David Zeko, Earth, Ocean and Atmospheric Sciences, University of British Columbia, Vancouver, BC, Canada, dzeko@eoas.ubc.ca; Barbara Zihlmann, School of Ocean and Earth Science, University of Southampton, Southampton, UK, barbara.zihlmann@soton.ac.uk

## Data Availability Statement

Samples in Table S1 in Supporting Information S1 have IGSN numbers and locations. Data in Table S1 in Supporting Information S1 are in the process of being archived in the Geochron database (www.geochron.org). Figures 4 and 6 are compilations of images that are published at http://publications.iodp.org/other/Oman/OmanDP.html, where they are freely available, with more detailed references provided in the figure captions. Figures 1, 2 and 5, and 7–17, Figures S1 and S2 in Supporting Information S1, and Tables S1 and S2 in Supporting Information S1 constitute data that are original with this paper. The two data tables are freely available at the open access Zenodo repository (https://zenodo.org/record/5736552#.YaVJxPHMLUI).

## References

Abers, G. A., MacKenzie, L. S., Rondenay, S., Zhang, Z., Wech, A. G., & Creager, K. C. (2009). Imaging the source region of Cascadia tremor and intermediate-depth earthquakes. *Geology*, *37*, 1119–1122. https://doi.org/10.1130/g30143a.1

Abers, G. A., Nakajima, J., vanKeken, P. E., Kita, S., & Hacker, B. R. (2013). Thermal-petrological controls on the location of earthquakes within subducting plates. *Earth and Planetary Science Letters*, *369–370*, 178–187. https://doi.org/10.1016/j.epsl.2013.03.022

Abu-Jaber, N. S., & Kimberley, M. M. (1992). Origin of ultramafic-hosted vein magnesite deposits. *Ore Geology Reviews*, *7*, 155–191. https://doi.org/10.1016/0169-1368(92)90004-5

Aftabi, A., & Zarrinkoub, M. H. (2013). Petrogeochemistry of listvenite association in metaophiolites of Sahlabad region, eastern Iran: Implications for possible epigenetic Cu-Au ore exploration in metaophiolites. *Lithos*, *156*, 186–203. https://doi.org/10.1016/j.lithos.2012.11.006

Agard, P., Yamato, P., Soret, M., Prigent, C., Guillot, S., Plunder, A., et al. (2016). Plate interface rheological switches during subduction infancy: Control on slab penetration and metamorphic sole formation. *Earth and Planetary Science Letters*, *451*, 208–220. https://doi.org/10.1016/j.epsl.2016.06.054

Akbulut, M., Piskin, O., & Karayigit, A. I. (2006). The genesis of the carbonatized and silicified ultramafics known as listvenites: A case study from the Mihaliccik region (Eskisehir), NW Turkey. *Geological Journal*, *41*, 557–580. https://doi.org/10.1002/gj.1058

Alabaster, T., Pearce, J. A., & Malpas, J. (1982). The volcanic stratigraphy and petrogenesis of the Oman ophiolite complex. *Contributions to Mineralogy and Petrology*, *81*, 168–183. https://doi.org/10.1007/bf00371294

Al Khirbash, S. (2015). Genesis and mineralogical classification of Ni-laterites, Oman Mountains. *Ore Geology Reviews*, *65*, 199–212. https://doi.org/10.1016/j.oregeorev.2014.09.022

Allegre, C. J., Montigny, R., & Bottinga, Y. (1973). Cortège ophiolitique et cortège océanique, géochimie comparée et mode de genèse. *Bulletin de la Société Géologique de France*, *7*, 461–477.

Alsharan, A. S., & Nasir, S. J. Y. (1996). Sedimentological and geochemical interpretation of a transgressive sequence: The Late Cretaceous Oahlah formation in the western Oman Mountains, United Arab Emirates. *Sedimentary Geology*, *101*, 227–242.

Amri, I., Ceuleneer, G., Benoit, M., Python, M., Puga, E., & Targuisti, K. (2007). Genesis of granitoids by interaction between mantle peridotites and hydrothermal fluids in oceanic spreading setting in the Oman ophiolite. *Geogaceta*, *42*, 23–26.

Andreani, M., Baronnet, A., Boullier, A.-M., & Gratier, J.-P. (2004). A microstructural study of a "crack-seal" type serpentine vein using SEM and TEM techniques. *European Journal of Mineralogy*, *16*, 585–595. https://doi.org/10.1127/0935-1221/2004/0016-0585

Arisi Rota, F., Brondi, A., Dessau, G., Branzini, M., Stea, B., & Vighi, L. (1971). I giacimenti minerari. In ''La Toscana Meridionale. Fondamenti geologico-minerari per una prospettiva di valorizzazione delle risorse naturali''. *Rendiconti della Società Italiana di Mineralogia e Petrologia*, *27*, 357–544.

Asimow, P. D., Dixon, J. E., & Langmuir, C. H. (2004). A hydrous melting and fractionation model for mid-ocean ridge basalts: Application to the Mid-Atlantic Ridge near the Azores. *Geochemistry, Geophysics, Geosystems*, *5*. https://doi.org/10.1029/2003gc000568

Bailey, E. H. (1981). Geologic map of Muscat-Ibra area, Sultanate of Oman. *Journal of Geophysical Research*, *86*. pocket map.

Barnes, I., O'Neill, J. R., Rapp, J. B., & White, D. E. (1973). Silica-carbonate alteration of serpentine: Wall rock alteration in mercury deposits of the California Coast Ranges. *Economic Geology*, *68*, 388–398. https://doi.org/10.2113/gsecongeo.68.3.388

Béchennec, F., Le Metour, J., Rabu, D., Bourdillon-de-Grissac, C., De Wever, P., Beurrier, M., & Villey, M. (1990). The Hawasina nappes: Stratigraphy, palaeogeography and structural evolution of a fragment of the south-Tethyan passive continental margin. *Geological Society, London, Special Publications*, *49*, 213–223. https://doi.org/10.1144/gsl.sp.1992.049.01.14

Béchennec, F., Le Métour, J., Rabu, D., Villey, M., & Beurrier, M. (1988). The Hawasina basin: A fragment of a starved passive continental margin, thrust over the Arabian platform during obduction of the Sumail nappe. *Tectonophysics*, *151*, 323–343. https://doi.org/10.1016/0040-1951(88)90251-x

Beinlich, A., Austrheim, H., Glodny, J., Erambert, M., & Andersen, T. B. (2010). $CO_2$ sequestration and extreme Mg depletion in serpentinized peridotite clasts from the Devonian Solund basin, SW-Norway. *Geochimica et Cosmochimica Acta*, *74*, 6935–6964. https://doi.org/10.1016/j.gca.2010.07.027

Beinlich, A., Plümper, O., Boter, E., Müller, I. A., Kourim, F., Ziegler, M., et al. (2020). Oman drilling project science TeamUltramafic rock carbonation: Constraints from listvenite core BT1B, Oman drilling project. *Journal of Geophysical Research*, *125*, e2019JB019060. https://doi.org/10.1029/2019jb019060

Benoit, M., Ceuleneer, G., & Polvé, M. (1999). The remelting of hydrothermally altered peridotite at mid-ocean ridges by intruding mantle diapirs. *Nature*, *402*, 514–518. https://doi.org/10.1038/990073

Berman, R. G. (1988). Internally-consistent thermodynamic data for minerals in the system $Na_2O$-$K_2O$-$CaO$-$MgO$-$FeO$-$Fe_2O_3$-$Al_2O_3$-$SiO_2$-$TiO_2$-$H_2O$-$CO_2$. *Journal of Petrology*, *29*, 445–522. https://doi.org/10.1093/petrology/29.2.445

Borojević Šoštarić, S., Palinkaš, A. L., Neubauer, F., Cvetković, V., Bernroider, M., & Genser, J. (2014). The origin and age of the metamorphic sole from the Rogozna Mts., Western Vardar Belt: New evidence for the one-ocean model for the Balkan ophiolites. *Lithos*, *192*, 39–55.

Boschi, C., Dini, A., Dallai, L., Ruggieri, G., & Gianelli, G. (2009). Enhanced $CO_2$-mineral sequestration by cyclic hydraulic fracturing and Si-rich fluid infiltration into serpentinites at Malentrata (Tuscany, Italy). *Chemical Geology*, *265*, 209–226. https://doi.org/10.1016/j.chemgeo.2009.03.016

Bottinga, Y., & Allegre, C. J. (1973). Thermal aspects of sea-floor spreading and the nature of the oceanic crust. *Tectonophysics*, *18*, 1–17. https://doi.org/10.1016/0040-1951(73)90075-9

Boudier, F., Ceuleneer, G., & Nicolas, A. (1988). Shear zones, thrusts and related magmatism in the Oman ophiolite: Initiation of thrusting on an oceanic ridge. *Tectonophysics*, *151*, 275–296. https://doi.org/10.1016/0040-1951(88)90249-1

Boudier, F., & Coleman, R. G. (1981). Cross section through the peridotite in the Semail ophiolite. *Journal of Geophysical Research*, *86*, 2573–2592. https://doi.org/10.1029/jb086ib04p02573

Braun, M. G., & Kelemen, P. B. (2002). Dunite distribution in the Oman ophiolite: Implications for melt flux through porous dunite conduits. *Geochemistry, Geophysics, Geosystems*, *3*. https://doi.org/10.1029/2001gc000289

Breton, J.-P., Béchennec, F., Le Métour, J., Moen-Maurel, L., & Razin, P. (2004). Eoalpine (Cretaceous) evolution of the Oman Tethyan continental margin: Insights from a structural field study in Jabal Akhdar (Oman Mountains). *GeoArabia*, *9*, 41–58. https://doi.org/10.2113/geoarabia090241

Briqueu, L., Mével, C., & Boudier, F. (1991). Sr, Nd and Pb isotopic constraints on the genesis of a calc-alkaline plutonic suite in the Oman Mountains related to the obduction process. In T. Peters, A. Nicolas, & R. G. Coleman (Eds.), *Ophiolite genesis and evolution of the oceanic lithosphere* (pp. 517–542). Muscat, Oman: Ministry of Petroleum and Minerals, Sultanate of Oman. https://doi.org/10.1007/978-94-011-3358-6_26

Carmichael, D. M. (1987). Induced stress and secondary mass transfer: Thermodynamic basis for the tendency toward constant-volume constraint in diffusion metasomatism. In H. C. Helgeson (Ed.), *Chemical transport in metasomatic processes, NATO ASI Series C, 218* (pp. 239–264). Dordrecht: Springer. https://doi.org/10.1007/978-94-009-4013-0_10

Chemenda, A. I., Burg, J.-P., & Mattauer, M. (2000). Evolutionary model of the Himalaya-Tibet system: Geopoem based on new modelling, geological and geophysical data. *Earth and Planetary Science Letters*, *174*, 397–409. https://doi.org/10.1016/s0012-821x(99)00277-0

Christensen, N. L., & Smewing, J. D. (1981). Geology and seismic structure of the sorthern section of the Oman ophiolite. *Journal of Geophysical Research*, *86*, 2545–2555. https://doi.org/10.1029/jb086ib04p02545

Coleman, R. G., & Hopson, C. A. (Eds.). (1981). Oman ophiolite special issue. *Journal of Geophysical Research*, *86*, 2495–2782.

Coleman, R. G., Keith, T. E. (1971). Chemical study of serpentinization—Burro Mountain, California. *Journal of Petrology*, *12*, 311. https://doi.org/10.1093/petrology/12.2.311

Connolly, J. A. D. (1990). Multivariable phase-diagrams—An algorithm based on generalized thermodynamics. *American Journal of Science*, *290*, 666–718. https://doi.org/10.2475/ajs.290.6.666

Connolly, J. A. D. (2005). Computation of phase equilibria by linear programming: A tool for geodynamic modeling and its application to subduction zone decarbonation. *Earth and Planetary Science Letters*, *236*, 524–541. https://doi.org/10.1016/j.epsl.2005.04.033

Connolly, J. A. D. (2009). The geodynamic equation of state: What and how. *Geochemistry, Geophysics, Geosystems*, *10*, Q10014. https://doi.org/10.1029/2009GC002540

Cooper, D. J. W. (1988). Structure and sequence of thrusting in deep-water sediments during ophiolite emplacement in the south-central Oman Mountains. *Journal of Structural Geology*, *10*, 473–485. https://doi.org/10.1016/0191-8141(88)90035-1

Cooperdock, E. H. G., Stockli, D. F., Kelemen, P. B., & de Obeso, J. C. (2020). Timing of magnetite growth associated with peridotite-hosted carbonate veins in the SE Samail ophiolite, Wadi fins, Oman. *Journal of Geophysical Research: Solid Earth*, *125*(5), e2019JB018632. https://doi.org/10.1029/2019jb018632

Cowan, R. J., Searle, M. P., & Waters, D. J. (2014). Structure of the metamorphic sole to the Oman ophiolite, Sumeini window and Wadi Tayyin: Implications for ophiolite obduction processes. *Geological Society, London, Special Publications*, *392*, 155–175. https://doi.org/10.1144/sp392.8

Cox, J., Searle, M., & Pedersen, R. (1999). The petrogenesis of leucogranitic dykes intruding the northern Semail ophiolite, United Arab Emirates: Field relationships, geochemistry and Sr/Nd isotope systematics. *Contributions to Mineralogy and Petrology*, *137*, 267–287. https://doi.org/10.1007/s004100050550

de Obeso, J. C., & Kelemen, P. B. (2018). Fluid rock interactions in residual mantle peridotites overlain by shallow oceanic limestones: Insights from Wadi Fins, Sultanate of Oman. *Chemical Geology*, *498*, 139–149. https://doi.org/10.1016/j.chemgeo.2018.09.022

de Obeso, J. C., Kelemen, P. B., Leong, J. A., Menzel, M. D., Manning, C. E., Godard, M., et al. (2022). Deep sourced fluids for peridotite carbonation in the shallow mantle wedge of a fossil subduction zone: Sr and C isotope profiles of OmanDP Hole BT1B. *Journal of Geophysical Research*, *127*(1), e2021JB022704. https://doi.org/10.1029/2021jb022704

de Obeso, J. C., Santiago Ramos, D., Higgins, J., & Kelemen, P. (2021). A Mg isotopic perspective on the mobility of magnesium during serpentinization and carbonation of the Oman ophiolite. *Journal of Geophysical Research*, *126*, e2020JB020237. https://doi.org/10.1029/2020jb020237

Deines, P. (2002). The carbon isotope geochemistry of mantle xenoliths. *Earth-Science Reviews*, *58*, 247–278. https://doi.org/10.1016/s0012-8252(02)00064-8

Duncan, R. A. (1982). A captured island chain in the Coast Range of Oregon and Washington. *Journal of Geophysical Research*, *87*, 10827–10837. https://doi.org/10.1029/jb087ib13p10827

Durney, D. W., & Ramsay, J. G. (1973). Incremental strain measured by syntectonic crystallization growths. In K. A. De Jong & R. Scholten (Eds.), *Gravity and tectonics* (pp. 67–96). New York: John Wiley.

Ece Öi, M. O., Çoban, F., & Coban, F. (2005). Genesis of hydrothermal stockwork-type magnesite deposits associated with ophiolite complexes in the Kütahya-Eskişehir region, Turkey. *Neues Jahrbuch für Mineragie-Abhandlungen*, *181*, 191–205. https://doi.org/10.1127/0077-7757/2005/0014

Ernewein, M., Pflumio, C., & Whitechurch, H. (1988). The death of an accretion zone as evidenced by the magmatic history of the Sumail ophiolite (Oman). *Tectonophysics*, *151*, 247–274. https://doi.org/10.1016/0040-1951(88)90248-x

Escayola, M. P., Proenza, J. A., van Staal, C., Rogers, N., & Skulski, T. (2009). The Point Rousse listvenites, Baie Verte, Newfoundland: Altered ultramafic rocks with potential for gold mineralization? *Current Research, Newfoundland & Labrador Department of Natural Research*, *09–1*, 1–12.

Facq, S., Daniel, I., Montagnac, G., Cardon, H., & Sverjensky, D. A. (2016). Carbon speciation in saline solutions in equilibrium with aragonite at high pressure. *Chemical Geology*, *431*, 44–53. https://doi.org/10.1016/j.chemgeo.2016.03.021

Falk, E. S. (2014). *Carbonation of peridotite in the Oman ophiolite* (233 pp.). New York, NY: Columbia University.

Falk, E. S., & Kelemen, P. B. (2015). Geochemistry and petrology of listvenite in the Oman ophiolite: Complete carbonation of peridotite during ophiolite emplacement. *Geochimica et Cosmochimica Acta*, *160*, 70–90. https://doi.org/10.1016/j.gca.2015.03.014

Farley, K. A. (2002). (U-Th)/He dating: Techniques, calibrations, and applications. *Reviews in Mineralogy and Geochemistry*, *47*(1), 819-844. https://doi.org/10.2138/rmg.2002.47.18

Farley, K. A., Wolf, R. A., & Silver, L. T. (1996). The effects of long alpha-stopping distances on (U-Th)/He ages. *Geochimica et Cosmochimica Acta*, *60*(21), 4223–4229. https://doi.org/10.1016/s0016-7037(96)00193-7

Fletcher, R. C., & Merino, E. (2001). Mineral growth in rocks: Kinetic-rheological models of replacement, vein formation, and syntectonic crystallization. *Geochimica et Cosmochimica Acta*, *65*, 3733–3748. https://doi.org/10.1016/s0016-7037(01)00726-8

Foley, S. F., & Fischer, T. P. (2017). An essential role for continental rifts and lithosphere in the deep carbon cycle. *Nature Geoscience*, *10*, 897–902. https://doi.org/10.1038/s41561-017-0002-7

Francis, G. H. (1956). The serpentinite mass in glen Urquhart, Inverness-shire, Scotland. *American Journal of Science*, *254*, 201–226. https://doi.org/10.2475/ajs.254.4.201

Garber, J. M., Rioux, M., Kylander-Clark, A. R., Hacker, B. R., Vervoort, J. D., & Searle, M. P. (2020). Petrochronology of Wadi Tayin metamorphic sole metasediment, with implications for the thermal and tectonic evolution of the Samail ophiolite (Oman/UAE). *Tectonics*, *39*, e2020TC006135. https://doi.org/10.1029/2020tc006135

Garcia del Real, P., Maher, K., Kluge, T., Bird, D. K., Brown, G. E., & John, C. M. (2016). Clumped-isotope thermometry of magnesium carbonates in ultramafic rocks. *Geochimica et Cosmochimica Acta*, *193*, 222–250. https://doi.org/10.1016/j.gca.2016.08.003

Gerbert-Gaillard, L. (2002). *Caractérisation Géochimique des Péridotites de l'ophiolite d'Oman: Processus magmatiques aux limites lithosphère/asthenosphere* (241 pp). Montpellier, FR: Université Montpellier II—Sciences et Techniques du Languedoc.

Ghent, E. D., & Stout, M. Z. (1981). Metamorphism at the base of the Samail ophiolite, southeastern Oman Mountains. *Journal of Geophysical Research*, *86*, 2557–2571. https://doi.org/10.1029/jb086ib04p02557

Glennie, K. W., Boeuf, M. G. A., Hughes-Clarke, M. W., Moody-Stuart, M., Pilaar, W. F. H., & Reinhardt, B. M. (1973). Late Cretaceous nappes in the Oman Mountains and their geologic evolution. *American Association of Petroleum Geologists Bulletin*, *57*, 5–27. https://doi.org/10.1306/819a4240-16c5-11d7-8645000102c1865d

Glennie, K. W., Boeuf, M. G. A., Hughes-Clarke, M. W., Moody-Stuart, M., Pilaar, W. F. H., & Reinhardt, B. M. (1974). Geology of the Oman Mountains. *Verhandelingen Koninklijk Nederlands Geologisch-Mijnbouwkundig Genootschap*, *31*, 1–423.

Godard, M., Carter, E. J., Decrausaz, T., Lafay, R., Bennett, E., Kourim, F., et al. (2021). Geochemical Profiles Across the Listvenite-Metamorphic Transition in the Basal Megathrust of the Semail Ophiolite: Results From Drilling at OmanDP Hole BT1B. *Journal of Geophysical Research: Solid Earth*, *126*(12), e2021JB022733. https://doi.org/10.1029/2021jb022733

Godard, M., Jousselin, D., & Bodinier, J.-L. (2000). Relationships between geochemistry and structure beneath a palaeo-spreading centre: A study of the mantle section in the Oman ophiolite. *Earth and Planetary Science Letters*, *180*, 133–148. https://doi.org/10.1016/s0012-821x(00)00149-7

Gottschalk, M. (1996). Internally consistent thermodynamic data for rock-forming minerals in the system $SiO_2$-$TiO_2$-$Al_2O_3$-$Fe_2O_3$-CaO-MgO-FeO-$K_2O$-$Na_2O$-$H_2O$-$CO_2$. *European Journal of Mineralogy*, *9*(1), 175–223. https://doi.org/10.1127/ejm/9/1/0175

Green, D. H. (1961). Ultramafic breccias from the Musa Valley, eastern Papua. *Geological Magazine*, *98*, 1–26. https://doi.org/10.1017/s0016756800000030

Green, D. H. (1964). The petrogenesis of the high-temperature peridotite intrusion in the Lizard area, Cornwall. *Journal of Petrology*, *5*, 134–188. https://doi.org/10.1093/petrology/5.1.134

Gregory, R. T., & Taylor, H. P., Jr (1981). An oxygen isotope profile in a section of Cretaceous oceanic crust, Samail ophiolite, Oman: Evidence for δ18O buffering of the oceans by deep (>5 km) seawater-hydrothermal circulation at mid-ocean ridges. *Journal of Geophysical Research*, *86*, 2737–2755. https://doi.org/10.1029/jb086ib04p02737

Grobe, A., Virgo, S., von Hagke, C., Urai, J. L., & Littke, R. (2018). Multiphase structural evolution of a continental margin during obduction orogeny: Insights from the Jebel Akhdar dome, Oman Mountains. *Tectonics*, *37*, 888–913. https://doi.org/10.1002/2016tc004442

Grobe, A., von Hagke, C., Littke, R., Dunkl, I., Wübbeler, F., Muchez, P., & Urai, J. L. (2019). Tectono-thermal evolution of Oman's Mesozoic passive continental margin under the obducting Semail ophiolite: A case study of Jebel Akhdar, Oman. *Solid Earth*, *10*, 149–175. https://doi.org/10.5194/se-10-149-2019

Guilmette, C., Smit, M. A., van Hinsbergen, D. J. J., Gürer, D., Corfu, F., Charette, B., et al. (2018). Forced subduction initiation recorded in the sole and crust of the Semail ophiolite of Oman. *Nature Geoscience*, *11*, 699–705. https://doi.org/10.1038/s41561-018-0209-2

Haase, K. M., Freund, S., Beier, C., Koepke, J., Erdmann, M., & Hauff, F. (2016). Constraints on the magmatic evolution of the oceanic crust from plagiogranite intrusions in the Oman ophiolite. *Contributions to Mineralogy and Petrology*, *171*, 1–16. https://doi.org/10.1007/s00410-016-1261-9

Haase, K. M., Freund, S., Koepke, J., Hauff, F., & Erdmann, M. (2015). Melts of sediments in the mantle wedge of the Oman ophiolite. *Geology*, *43*, 275–278. https://doi.org/10.1130/g36451.1

Hacker, B. R. (1996). Eclogite formation and the rheology, buoyancy, seismicity, and $H_2O$ content of oceanic crust. *AGU Monograph*, *96*, 337–346. https://doi.org/10.1029/GM096p0337

Hacker, B. R. (2006). Pressures and temperatures of ultrahigh-pressure metamorphism: Implications for UHP tectonics and $H_2O$ in subducting slabs. *International Geology Review*, *48*, 1053–1066. https://doi.org/10.2747/0020-6814.48.12.1053

Hacker, B. R., & Gnos, E. (1997). The conundrum of Samail: Explaining the metamorphic history. *Tectonophysics*, *279*, 215–226. https://doi.org/10.1029/GM096p0337

Hacker, B. R., & Mosenfelder, J. L. (1996). Metamorphism and deformation along the emplacement thrust of the Samail ophiolite, Oman. *Earth and Planetary Science Letters*, *144*, 435–451. https://doi.org/10.1016/s0012-821x(96)00186-0

Hacker, B. R., Mosenfelder, J. L., & Gnos, E. (1996). Rapid emplacement of the Oman ophiolite: Thermal and geochronologic constraints. *Tectonics*, *15*, 1230–1247. https://doi.org/10.1029/96tc01973

Halls, C., & Zhao, R. (1995). Listvenite and related rocks: Perspectives on terminology and mineralogy with reference to an occurrence at Creg-ganbaun, Co. Mayo, Republic of Ireland. *Mineralium Deposita*, *30*, 303–313. https://doi.org/10.1007/bf00196366

Hanghoj, K., Kelemen, P. B., Hassler, D., & Godard, M. (2010). Composition and genesis of depleted mantle peridotites from the Wadi Tayin massif, Oman ophiolite: Major and trace element geochemistry, and Os isotope and PGE systematics. *Journal of Petrology*, *51*, 201–227. https://doi.org/10.1093/petrology/egp077

Hansen, L. D., Dipple, G. M., Gordon, T. M., & Kellett, D. A. (2005). Carbonated serpentinite (listwanite) at Atlin, British Columbia: A geological analogue to carbon dioxide sequestration. *The Canadian Mineralogist*, *43*, 225–239. https://doi.org/10.2113/gscanmin.43.1.225

Hansman, R. J., Ring, U., Thomson, S. N., den Brok, B., & Stübner, K. (2017). Late Eocene uplift of the Al Hajar Mountains, Oman, supported by stratigraphy and low-temperature thermochronology. *Tectonics*, *36*, 3081–3109. https://doi.org/10.1002/2017tc004672

Helgeson, H. C. (1985). Errata II. Thermodynamics of minerals, reactions, and aqueous solutions at high pressures and temperature. *American Journal of Science*, 8450855. *285*. https://doi.org/10.2475/ajs.285.9.845

Helgeson, H. C., Delany, J. M., Nesbitt, H. W., & Bird, D. K. (1978). Summary and critique of the thermodynamic properties of rock-forming minerals. *American Journal of Science*, *278-A*, 1–229. http://earth.geology.yale.edu/~ajs/1978/ajs_278A_1.pdf/1.pdf

Helgeson, H. C., Kirkham, D. H., & Flowers, G. C. (1981). Theoretical prediction of the thermodynamic behavior of aqueous electrolytes by high pressures and temperatures: IV, calculation of activity coefficients, osmotic coefficients, and apparent molal and standard and relative partial molal properties to 600 degrees C and 5kb. *American Journal of Science*, *281*, 1249–1516. https://doi.org/10.2475/ajs.281.10.1249

Herwegh, M., Mercolli, I., Linckens, J., & Müntener, O. (2016). Mechanical anisotropy controls strain localization in upper mantle shear zones. *Tectonics*, *35*, 1177–1204. https://doi.org/10.1002/2015tc004007

Hirose, F., Nakajima, J., & Hasegawa, A. (2008). Three-dimensional seismic velocity structure and configuration of the Philippine Sea slab in southwestern Japan estimated by double-difference tomography. *Journal of Geophysical Research*, *113*. https://doi.org/10.1029/2007JB005274

Holland, T., & Powell, R. (2003). Activity-composition relations for phases in petrological calculations: An asymmetric multicomponent formulation. *Contributions to Mineralogy and Petrology*, *145*, 492–501. https://doi.org/10.1007/s00410-003-0464-z

Holland, T. J. B., & Powell, R. (1998). An internally consistent thermodynamic data set for phases of petrological interest. *Journal of Metamorphic Geology*, *16*(3), 309–343. https://doi.org/10.1111/j.1525-1314.1998.00140.x

Horita, J. (2014). Oxygen and carbon isotope fractionation in the system dolomite-water-$CO_2$ to elevated temperatures. *Geochimica et Cosmochimica Acta*, *129*, 11–124. https://doi.org/10.1016/j.gca.2013.12.027

Huang, F., & Sverjensky, D. A. (2019). Extended Deep Earth Water Model for predicting major element mantle metasomatism. *Geochimica et Cosmochimica Acta*, *254*, 192–230. https://doi.org/10.1016/j.gca.2019.03.027

Ishikawa, T., Nagaishi, K., & Umino, S. (2002). Boninitic volcanism in the Oman ophiolite: Implications for thermal condition during transition from spreading ridge to arc. *Geology*, *30*, 899–902. https://doi.org/10.1130/0091-7613(2002)030<0899:bvitoo>2.0.co;2

Jamtveit, B., Putnis, C., & Malthe-Sorenssen, A. (2009). Reaction induced fracturing during replacement processes. *Contributions to Mineralogy and Petrology*, *157*, 127–133. https://doi.org/10.1007/s00410-008-0324-y

Johnson, J. W., Oelkers, E. H., & Helgeson, H. C. (1992). SUPCRT92-A software package for calculating the standard molal thermodynamic properties of minerals, gases, aqueous species, and reactions from 1-bar to 5000-bar and 0°C to 1000°C. *Computers & Geosciences*, *18*, 899–947. https://doi.org/10.1016/0098-3004(92)90029-q

Jurković, I., Palinkaš, L. A., Garašić, V., & Strmić Palinkaš, S. (2012). Genesis of vein-stockwork cryptocrystalline magnesite from the Dinaride ophiolites. *Ophioliti*, *37*, 13–26.

Kelemen, P. B., Braun, M., & Hirth, G. (2000). Spatial distribution of melt conduits in the mantle beneath oceanic spreading ridges: Observations from the Ingalls and Oman ophiolites. *Geochemistry, Geophysics, Geosystems*, *1*. https://doi.org/10.1029/1999gc000012

Kelemen, P. B., Evans, O., Ghiorso, M., Mustard, J., Ehlmann, B. L., Spiegelman, M. (2020). Carbonate in olivine-rich unit (s) on Mars may have formed at low P ($H_2O$). *Lunar & Planetary Science Conference Abstracts*, *1213*.

Kelemen, P. B., & Hirth, G. (2012). Reaction-driven cracking during retrograde metamorphism: Olivine hydration and carbonation. *Earth and Planetary Science Letters*, *345–348*, 81–89. https://doi.org/10.1016/j.epsl.2012.06.018

Kelemen, P. B., Koga, K., & Shimizu, N. (1997). Geochemistry of gabbro sills in the crust-mantle transition zone of the Oman ophiolite: Implications for the origin of the oceanic lower crust. *Earth and Planetary Science Letters*, *146*, 475–488. https://doi.org/10.1016/s0012-821x(96)00235-x

Kelemen, P. B., Leong, J. A., Carlos de Obeso, J., Matter, J. M., Ellison, E. T., Templeton, A., et al. (2021). Initial Results From the Oman Drilling Project Multi-Borehole Observatory: Petrogenesis and Ongoing Alteration of Mantle Peridotite in the Weathering Horizon. *Journal of Geophysical Research: Solid Earth*, *126*(12). https://doi.org/10.1029/2021jb022729

Kelemen, P. B., & Manning, C. E. (2015). Reevaluating carbon fluxes in subduction zones: What goes down, mostly comes up. *Proceedings of the National Academy of Sciences*, *112*, E3997–E4006. https://doi.org/10.1073/pnas.1507889112

Kelemen, P. B., Matter, J. M., Teagle, D. A. H., Coggon, J. A., & Oman Drilling Project Science Team. (2020). Site BT1: Fluid and mass exchange on a subduction zone plate boundary. In P. B. Kelemen, J. M. Matter, D. A. H. Teagle, J. A. Coggon (Eds.), & Oman Drilling Project Science Team (Eds.), *Proceedings of the Oman drilling project*. International Ocean Discovery Program. https://doi.org/10.14379/Oman.ph1-2.proc.2020

Kelemen, P. B., Shimizu, N., & Salters, V. J. M. (1995). Extraction of mid-ocean-ridge basalt from the upwelling mantle by focused flow of melt in dunite channels. *Nature*, *375*(6534), 747–753. https://doi.org/10.1038/375747a0

Kerrick, D. M., & Connolly, J. A. D. (2001). Metamorphic devolatilization of subducted oceanic metabasalts: Implications for seismicity, arc magmatism and volatile recycling. *Earth and Planetary Science Letters*, *189*(1–2), 19–29. https://doi.org/10.1016/s0012-821x(01)00347-8

Kerrick, D. M., & Jacobs, G. K. (1981). A modified Redlich-Kwong equation for $H_2O$, $CO_2$, and $H_2O$-$CO_2$ mixtures at elevated pressures and temperatures. *American Journal of Science*, *281*(6), 735–767. https://doi.org/10.2475/ajs.281.6.735

Khedr, M. Z., Arai, S., & Python, M. (2013). Petrology and chemistry of basal lherzolites above the metamorphic sole from Wadi Sarami central Oman ophiolite. *Journal of Mineralogical and Petrological Sciences*, *108*(1), 13–24. https://doi.org/10.2465/jmps.121026

Khedr, M. Z., Arai, S., Python, M., & Tamura, A. (2014). Chemical variations of abyssal peridotites in the central Oman ophiolite: Evidence of oceanic mantle heterogeneity. *Gondwana Research*, *25*(3), 1242–1262. https://doi.org/10.1016/j.gr.2013.05.010

Klein, E. M., & Langmuir, C. H. (1987). Global correlations of ocean ridge basalt chemistry with axial depth and crustal thickness. *Journal of Geophysical Research*, *92*(B8), 8089–8115. https://doi.org/10.1029/jb092ib08p08089

Klein, F., & Garrido, C. J. (2011). Thermodynamic constraints on mineral carbonation of serpentinized peridotite. *Lithos*, *126*(3–4), 147–160. https://doi.org/10.1016/j.lithos.2011.07.020

Klein, F., & Le Roux, V. (2020). Quantifying the volume increase and chemical exchange during serpentinization. *Geology*, *48*(6), 552–556. https://doi.org/10.1130/g47289.1

Kotowski, A., Cloos, M., Stockli, D., & Orent, E. B. (2021). Structural and thermal evolution of an infant subduction shear zone: Insights from sub-ophiolite metamorphic rocks recovered from Oman Drilling Project Site BT-1B. *Journal of Geophysical Research*. Revised and in review, preprint. Retrieved from https://www.essoar.org/doi/10.1002/essoar.10505943.1

Lacinska, A. M., & Styles, M. T. (2013). Silicified serpentinite—A residuum of a Tertiary palaeo-weathering surface in the United Arab Emirates. *Geological Magazine*, *150*, 385–395.

Lafay, R., Godard, M., Menzel, M., Beinlich, A., Kourim, F., Decrausaz, T., & Oman Drilling Project Phase 1 Science Party. (2020). Listvenization processes in the mantle atop the Samail ophiolite metamorphic sole: Mineralogical and thermodynamic constraints. In *International conference on ophiolites and the oceanic lithosphere: Results of the Oman drilling project and related research, 12–14th, January, 2020, Sultan Qaboos University, Muscat, Sultanate of Oman*.

Lanphere, M. A., Coleman, R. G., & Hopson, C. A. (1981). Sr isotopic tracer study of the Samail ophiolite, Oman. *Journal of Geophysical Research: Solid Earth*, *86*(B4), 2709–2720. https://doi.org/10.1029/jb086ib04p02709

Lapham, D. M. (1961). New data on deweylite. *American Mineralogist*, *46*, 168–188.

Li, S.-G., Yang, W., Ke, S., Meng, X., Tian, H., Xu, L., et al. (2017). Deep carbon cycles constrained by a large-scale mantle Mg isotope anomaly in eastern China. *National Science Review*, *4*(1), 111–120. https://doi.org/10.1093/nsr/nww070

Linckens, J., Herwegh, M., Müntener, O., & Mercolli, I. (2011). Evolution of a polymineralic mantle shear zone and the role of second phases in the localization of deformation. *Journal of Geophysical Research*, *116*(B6). https://doi.org/10.1029/2010jb008119

Lippard, S. J., Shelton, A. W., & Gass, I. G. (1986). The ophiolite of northern Oman. *Geological Society London Memoirs*, *11*, 178. 178.

MacLeod, C. J., Johan Lissenberg, C., & Bibby, L. E. (2013). "Moist MORB" axial magmatism in the Oman ophiolite: The evidence against a mid-ocean ridge origin. *Geology*, *41*(4), 459–462. https://doi.org/10.1130/g33904.1

Malvoisin, B. (2015). Mass transfer in the oceanic lithosphere: Serpentinization is not isochemical. *Earth and Planetary Science Letters*, *430*, 75–85. https://doi.org/10.1016/j.epsl.2015.07.043

Malvoisin, B., Zhang, C., Müntener, O., Baumgartner, L. P., & Kelemen, P. B. (2020). Measurement of volume change and mass transfer during serpentinization: Insights from the oman drilling project. *Journal of Geophysical Research*, *125*(5). https://doi.org/10.1029/2019jb018877

McCulloch, M., Gregory, R., Wasserburg, G., & Taylor, H., Jr (1980). A neodymium, strontium, and oxygen isotopic study of the Cretaceous Samail ophiolite and implications for the petrogenesis and seawater-hydrothermal alteration of oceanic crust. *Earth and Planetary Science Letters*, *46*(2), 201–211. https://doi.org/10.1016/0012-821x(80)90006-0

McCulloch, M. T., Gregory, R. T., Wasserburg, G. J., & Taylor, H. P., Jr (1981). Sm-Nd, Rb-Sr, and 18O/16O isotopic systematics in an oceanic crustal section: Evidence from the Samail ophiolite. *Journal of Geophysical Research: Solid Earth*, *86*(B4), 2721–2735. https://doi.org/10.1029/jb086ib04p02721

McKenzie, D., & Bickle, M. J. (1988). The volume and composition of melt generated by extension of the lithosphere. *Journal of Petrology*, *29*(3), 625–679. https://doi.org/10.1093/petrology/29.3.625

Menzel, M. D., Garrido, C. J., López Sánchez-Vizcaíno, V., Marchesi, C., Hidas, K., Escayola, M. P., & Delgado Huertas, A. (2018). Carbonation of mantle peridotite by $CO_2$-rich fluids: The formation of listvenites in the advocate ophiolite complex (Newfoundland, Canada). *Lithos*, *323*, 238–261. https://doi.org/10.1016/j.lithos.2018.06.001

Menzel, M. D., Urai, J. L., de Obeso, J. C., Kotowski, A., Manning, C. E., Kelemen, P. B., et al. (2020). Brittle deformation of carbonated peridotite—Insights from listvenites of the Samail Ophiolite (Oman Drilling Project Hole BT1B). *Journal of Geophysical Research: Solid Earth*, *125*(10). https://doi.org/10.1029/2020jb020199

Menzel, M. D., Urai, J. L., Ukar, E., Hirth, G., Schwedt, A., Kovács, A., et al. (2021). Ductile deformation during carbonation of serpentinized peridotite. *Nature Communications*. revised and in review, preprint. Retrieved from https://eartharxiv.org/repository/object/2416/download/4961/

Monnier, C., Girardeau, J., Le Mée, L., & Polvé, M. (2006). Along-ridge petrological segmentation of the mantle in the Oman ophiolite. *Geochemistry, Geophysics, Geosystems*, *7*. https://doi.org/10.1029/2006GC001320

Nahon, D., & Merino, E. (1997). Pseudomorphic replacement in tropical weathering: Evidence, geochemical consequences, and kinetic-rheological origin. *American Journal of Science*, *297*(4), 393–417. https://doi.org/10.2475/ajs.297.4.393

Nasir, S., Al Sayigh, A. R., Al Harthy, A., Al-Khirbash, S., Al-Jaaidi, O., Musllam, A., et al. (2007). Mineralogical and geochemical characterization of listwaenite from the Semail ophiolite, Oman. *Geochemistry*, *67*(3), 213–228. https://doi.org/10.1016/j.chemer.2005.01.003

Nicolas, A., Boudier, F., & Ildefonse, B. (1996). Variable crustal thickness in the Oman ophiolite: Implication for oceanic crust. *Journal of Geophysical Research: Solid Earth*, *101*(B8), 17941–17950. https://doi.org/10.1029/96jb00195

Nicolas, A., Boudier, F., Ildefonse, B., & Ball, E. (2000). Accretion of Oman and United Arab Emirates ophiolite: Discussion of a new structural map. *Marine Geophysical Research*, *21*, 147–179.

Ninkabou, D., Agard, P., Nielsen, C., Smit, J., Gorini, C., Rodriguez, M., et al. (2021). Structure of the offshore obducted Oman margin: Emplacement of the Semail ophiolite and role of tectonic inheritance. *Journal of Geophysical Research: Solid Earth*, *126*(2). https://doi.org/10.1029/2020jb020187

Nolan, S. C., Skelton, P. W., Clissold, B. P., & Smewing, J. D. (1990). Maastrichtian to early Tertiary stratigraphy and palaeogeography of the central and northern Oman Mountains. *Geological Society, London, Special Publications*, *49*(1), 495–519. https://doi.org/10.1144/gsl.sp.1992.049.01.31

Okazaki, K., Michibayashi, K., Hatakeyama, K., Abe, N., Johnson, K. T. M., & Kelemen, P. B. (2021). Major mineral fraction and physical properties of carbonated peridotite (listvenite) from ICDP Oman Drilling Project Hole BT1B inferred from X-ray CT core images. *Journal of Geophysical Research: Solid Earth*, *26*(12). https://doi.org/10.1029/2021jb022719

Oskierski, H. C., Bailey, J. G., Kennedy, E. M., Jacobsen, G., Ashley, P. M., & Dlugogorski, B. Z. (2013). Formation of weathering-derived magnesite deposits in the New England Orogen, New South Wales, Australia: Implications from mineralogy, geochemistry and genesis of the Attunga magnesite deposit. *Mineralium Deposita*, *48*(4), 525–541. https://doi.org/10.1007/s00126-012-0440-5

Oskierski, H. C., Dlugogorski, B. Z., & Jacobsen, G. (2013). Sequestration of atmospheric $CO_2$ in a weathering-derived, serpentinite-hosted magnesite deposit: 14C tracing of carbon sources and age constraints for a refined genetic model. *Geochimica et Cosmochimica Acta*, *122*, 226–246. https://doi.org/10.1016/j.gca.2013.08.029

Pan, D., Spanu, L., Harrison, B., Sverjensky, D. A., & Galli, G. (2013). Dielectric properties of water under extreme conditions and transport of carbonates in the deep Earth. *Proceedings of the National Academy of Sciences*, *110*(17), 6646–6650. https://doi.org/10.1073/pnas.1221581110

Peacock, S. M. (1996). Thermal and petrologic structure of subduction zones. *AGU Monograph*, *96*, 119–133. https://doi.org/10.1029/GM096p0119

Peacock, S. M., van Keken, P. E., Holloway, S. D., Hacker, B. R., Abers, G. A., & Fergason, R. L. (2005). Thermal structure of the Costa Rica-Nicaragua subduction zone. *Physics of the Earth and Planetary Interiors*, *149*(1–2), 187–200. https://doi.org/10.1016/j.pepi.2004.08.030

Pearce, J. A., Alabaster, T., Shelton, A. W., & Searle, M. P. (1981). The Oman ophiolite as a Cretaceous arc-basin complex: Evidence and implications. *Philosophical Transactions of the Royal Society of London. Series A, Mathematical and Physical Sciences*, *300*(1454), 299–317. https://doi.org/10.1098/rsta.1981.0066

Pearce, J. A., & Peate, D. W. (1995). Tectonic implications of the composition of volcanic arc magmas. *Annual Review of Earth and Planetary Sciences*, *23*(1), 251–286. https://doi.org/10.1146/annurev.ea.23.050195.001343

Penniston-Dorland, S. C., Kohn, M. J., & Manning, C. E. (2015). The global range of subduction zone thermal structures from exhumed blueschists and eclogites: Rocks are hotter than models. *Earth and Planetary Science Letters*, *428*, 243–254. https://doi.org/10.1016/j.epsl.2015.07.031

Peuble, S., Godard, M., Gouze, P., Leprovost, R., Martinez, I., & Shilobreeva, S. (2019). Control of $CO_2$ on flow and reaction paths in olvine-dominated basements: An experimental study. *Geochimica et Cosmochimica Acta*, *252*, 16–38. https://doi.org/10.1016/j.gca.2019.02.007

Posukhova, T. V., Panasian, L. L., & Sas, I. E. (2013). Serpentinites of the ural: Mineralogical features, petrophysical properties and subduction processes. *Open Journal of Geology*. https://doi.org/10.4236/ojg.2013

Powell, R., Holland, T., & Worley, B. (1998). Calculating phase diagrams involving solid solutions via non-linear equations, with examples using THERMOCALC. *Journal of Metamorphic Geology*, *16*(4), 577–588. https://doi.org/10.1111/j.1525-1314.1998.00157.x

Prigent, C., Agard, P., Guillot, S., Godard, M., & Dubacq, B. (2018). Mantle wedge (de)formation during subduction infancy: Evidence from the base of the Semail ophiolitic mantle. *Journal of Petrology*, *59*(11), 2061–2092. https://doi.org/10.1093/petrology/egy090

Prigent, C., Guillot, S., Agard, P., Lemarchand, D., Soret, M., & Ulrich, M. (2018). Transfer of subduction fluids into the deforming mantle wedge during nascent subduction: Evidence from trace elements and boron isotopes (Semail ophiolite, Oman). *Earth and Planetary Science Letters*, *484*, 213–228. https://doi.org/10.1016/j.epsl.2017.12.008

Quesnel, B., Boulvais, P., Gautier, P., Cathelineau, M., John, C. M., Dierick, M., et al. (2016). Paired stable isotopes (O, C) and clumped isotope thermometry of magnesite and silica veins in the New Caledonia Peridotite Nappe. *Geochimica et Cosmochimica Acta*, *183*, 234–249. https://doi.org/10.1016/j.gca.2016.03.021

Quesnel, B., Gautier, P., Boulvais, P., Cathelineau, M., Maurizot, P., Cluzel, D., et al. (2013). Syn-tectonic, meteoric water-derived carbonation of the New Caledonia peridotite nappe. *Geology*, *41*(10), 1063–1066. https://doi.org/10.1130/g34531.1

Raleigh, C. B., & Paterson, M. S. (1965). Experimental deformation of serpentinite and its tectonic implications. *Journal of Geophysical Research*, *70*(16), 3965–3985. https://doi.org/10.1029/jz070i016p03965

Reiners, P. W., Spell, T. L., Nicolescu, S., & Zanetti, K. A. (2004). Zircon (U-Th)/He thermochronometry: He diffusion and comparisons with 40Ar/39Ar dating. *Geochimica et Cosmochimica Acta*, *68*(8), 1857–1887. https://doi.org/10.1016/j.gca.2003.10.021

Rioux, M., Benoit, M., Amri, I., Ceuleneer, G., Garber, J. M., Searle, M., & Leal, K. (2021). The origin of felsic intrusions within the mantle section of the Samail ophiolite: Geochemical evidence for three distinct mixing and fractionation trends. *Journal of Geophysical Research: Solid Earth*, *126*(5). https://doi.org/10.1029/2020jb020760

Rioux, M., Bowring, S., Kelemen, P., Gordon, S., Dudás, F., & Miller, R. (2012). Rapid crustal accretion and magma assimilation in the Oman-U.A.E. ophiolite: High precision U-Pb zircon geochronology of the gabbroic crust. *Journal of Geophysical Research*, *117*, B07201. https://doi.org/10.1029/2012JB009273

Rioux, M., Bowring, S., Kelemen, P., Gordon, S., Miller, R., & Dudás, F. (2013). Tectonic development of the Samail ophiolite: High-precision U-Pb zircon geochronology and Sm-Nd isotopic constraints on crustal growth and emplacement. *Journal of Geophysical Research: Solid Earth*, *118*(5), 2085–2101. https://doi.org/10.1002/jgrb.50139

Rioux, M., Garber, J., Bauer, A., Bowring, S., Searle, M., Kelemen, P., & Hacker, B. (2016). Synchronous formation of the metamorphic sole and igneous crust of the Semail ophiolite: New constraints on the tectonic evolution during ophiolite formation from high-precision U–Pb zircon geochronology. *Earth and Planetary Science Letters*, *451*, 185–195. https://doi.org/10.1016/j.epsl.2016.06.051

Rioux, M., Garber, J. M., Searle, M., Kelemen, P., Miyashita, S., Adachi, Y., & Bowring, S. (2021). High-precision U-Pb zircon dating of late magmatic in the Samail ophiolite: A record of subduction initiation. *Journal of Geophysical Research: Solid Earth*, *126*(5). https://doi.org/10.1029/2020jb020758

Robertson, A. H. F., & Searle, M. P. (1990). The northern Oman Tethyan continental margin: Stratigraphy, structure, concepts and controversies. *Geological Society, London, Special Publications*, *49*(1), 3–25. https://doi.org/10.1144/gsl.sp.1992.049.01.02

Rollinson, H. (2015). Slab and sediment melting during subduction initiation: Granitoid dykes from the mantle section of the Oman ophiolite. *Contributions to Mineralogy and Petrology*, *170*. https://doi.org/10.1007/s00410-015-1177-9

Rudge, J. F., Kelemen, P. B., & Spiegelman, M. (2010). A simple model of reaction-induced cracking applied to serpentinization and carbonation of peridotite. *Earth and Planetary Science Letters*, *291*(1–4), 215–227. https://doi.org/10.1016/j.epsl.2010.01.016

Scambelluri, M., Bebout, G. E., Belmonte, D., Gilio, M., Campomenosi, N., Collins, N., & Crispini, L. (2016). Carbonation of subduction-zone serpentinite (high-pressure ophicarbonate; Ligurian Western Alps) and implications for the deep carbon cycling. *Earth and Planetary Science Letters*, *441*, 155–166. https://doi.org/10.1016/j.epsl.2016.02.034

Scarsi, M., Malatesta, C., & Fornasaro, S. (2018). Lawsonite-bearing eclogite from a tectonic mélange in the Ligurian Alps: New constraints for the subduction plate-interface evolution. *Geological Magazine*, *155*(2), 280–297. https://doi.org/10.1017/s0016756817000395

Scharf, A., Mattern, F., Bolhar, R., Bailey, C. M., & Ring, U. (2020). U-Pb dating of postobductional carbonate veins in listwaenite of the Oman Mountains near Fanja. Presented at Proceedings of the International Conference on Ophiolites and the Oceanic Lithosphere: Results of the Oman Drilling Project and Related Research, Sultan Qaboos University, Oman.

Schlüter, M., Steuber, T., Parente, M., & Mutterlose, J. (2008). Evolution of a Maastrichtian-Paleocene tropical shallow-water carbonate platform (Qalhat, NE Oman). *Facies*, *54*(4), 513–527. https://doi.org/10.1007/s10347-008-0150-8

Searle, M., & Cox, J. (1999). Tectonic setting, origin, and obduction of the Oman ophiolite. *Geological Society of America Bulletin*, *111*(1), 104–122. https://doi.org/10.1130/0016-7606(1999)111<0104:tsoaoo>2.3.co;2

Searle, M., & Cox, J. (2002). Subduction zone metamorphism during formation and emplacement of the Semail ophiolite in the Oman Mountains. *Geological Magazine*, *139*, 241–255. https://doi.org/10.1017/s0016756802006532

Searle, M. P., Lippard, S. J., Smewing, J. D., & Rex, D. C. (1980). Volcanic rocks beneath the Semail ophiolite nappe in the northern Oman Mountains and their significance in the Mesozoic evolution of Tethys. *Journal of the Geological Society London*, *137*(5), 589–604. https://doi.org/10.1144/gsjgs.137.5.0589

Searle, M. P., & Malpas, J. (1980). The structure and metamorphism of rocks beneath the Semail ophiolite of Oman and their significance in ophiolite obduction. *Transactions of the Royal Society of Edinburgh: Earth Sciences*, *71*(4), 247–262. https://doi.org/10.1017/s0263593300013614

Searle, M. P., & Malpas, J. (1982). Petrochemistry and origin of sub-ophiolitic metamorphic and related rocks in the Oman Mountains. *Journal of the Geological Society*, *139*(3), 235–248. https://doi.org/10.1144/gsjgs.139.3.0235

Searston, S. M. (1998). *Resource estimation and the Kunwarara magnesite deposit* (356 pp). University of Tasmania.

Shock, E. L., Oelkers, E. H., Johnson, J. W., Sverjensky, D. A., Helgeson, H. C. (1992). Calculation of the thermodynamic properties of aqueous species at high pressures and temperatures: Effective electrostatic radii, dissociation constants and standard partial molal properties to 1000°C and 5 kbar. *Journal of the Chemical Society, Faraday Transactions*, *88*(6), 803–826. https://doi.org/10.1039/ft9928800803

Shock, E. L., Sassani, D. C., Willis, M., & Sverjensky, D. A. (1997). Inorganic species in geologic fluids: Correlations among standard molal thermodynamic properties of aqueous ions and hydroxide complexes. *Geochimica et Cosmochimica Acta*, *61*(5), 907–950. https://doi.org/10.1016/s0016-7037(96)00339-0

Sofiya, A., Ishiwatari, A., Hirano, N., & Tsujimori, T. (2017). Relict chromian spinels in Tulu Dimtu serpentinites and listvenite, western Ethiopia: Implications for the timing of listvenite formation. *International Geology Review*, *59*(13), 1621–1631. https://doi.org/10.1080/00206814.2016.1213142

Soret, M., Agard, P., Dubacq, B., Plunder, A., & Yamato, P. (2017). Petrological evidence for stepwise accretion of metamorphic soles during subduction infancy (Semail ophiolite, Oman and UAE). *Journal of Metamorphic Geology*, *35*(9), 1051–1080. https://doi.org/10.1111/jmg.12267

Spencer, C. J., Cavosie, A. J., Raub, T. D., Rollinson, H., Jeon, H., Searle, M. P., et al. (2017). Evidence for melting mud in Earth's mantle from extreme oxygen isotope signatures in zircon. *Geology*, *45*(11), 975–978. https://doi.org/10.1130/g39402.1

Stanger, G. (1985). Silicified serpentinite in the Semail nappe of Oman. *Lithos*, *18*, 13–22. https://doi.org/10.1016/0024-4937(85)90003-9

Stewart, E. M., & Ague, J. J. (2020). Pervasive subduction zone devolatilization recycles $CO_2$ into the forearc. *Nature Communications*, *11*, 6220. https://doi.org/10.1038/s41467-020-19993-2

Styles, M. T., Ellison, R. A., Phillips, E. R., Arkley, S., Schofield, D. I., Thomas, R. J., et al. (2006). *The geology and geophysics of the United Arab Emirates* (Vol. 2, pp. 1–355). Ministry of Energy, United Arab Emirates.

Sverjensky, D. A., Harrison, B., & Azzolini, D. (2014). Water in the deep earth: The dielectric constant and the solubilities of quartz and corundum to 60 kb and 1200°C. *Geochimica et Cosmochimica Acta*, *129*, 125–145. https://doi.org/10.1016/j.gca.2013.12.019

Syracuse, E. M., van Keken, P. E., & Abers, G. A. (2010). The global range of subduction zone thermal models. *Physics of the Earth and Planetary Interiors*, *183*(1–2), 73–90. https://doi.org/10.1016/j.pepi.2010.02.004

Takazawa, E., Okayasu, T., & Satoh, K. (2003). Geochemistry and origin of the basal lherzolites from the northern Oman ophiolite (northern Fizh block). *Geochemistry, Geophysics, Geosystems*, *4*(2). https://doi.org/10.1029/2001gc000232

Tilton, G. R., Hopson, C. A., & Wright, J. E. (1981). Uranium-lead isotopic ages of the Samail ophiolite, Oman, with applications to Tethyan ocean ridge tectonics. *Journal of Geophysical Research: Solid Earth*, *86*(B4), 2763–2775. https://doi.org/10.1029/jb086ib04p02763

Ulrich, M., Munoz, M., Guillot, S., Cathelineau, M., Picard, C., Quesnel, B., et al. (2014). Dissolution-precipitation processes governing the carbonation and silicification of the serpentinite sole of the New Caledonia ophiolite. *Contributions to Mineralogy and Petrology*, *167*, 952. https://doi.org/10.1007/s00410-013-0952-8

Urai, J. L., Williams, P. F., & van Roermund, H. L. M. (1991). Kinematics of crystal growth in syntectonic fibrous veins. *Journal of Structural Geology*, *13*(7), 823–836. https://doi.org/10.1016/0191-8141(91)90007-6

van Hinsbergen, D. J. J., Maffione, M., Koornneef, L. M. T., & Guilmette, C. (2019). Kinematic and paleomagnetic restoration of the Semail ophiolite (Oman) reveals subduction initiation along an ancient Neotethyan fracture zone. *Earth and Planetary Science Letters*, *518*, 183–196. https://doi.org/10.1016/j.epsl.2019.04.038

van Keken, P. E., Wada, I., Sime, N., & Abers, G. A. (2019). Thermal structure of the forearc in subduction zones: A comparison of methodologies. *Geochemistry, Geophysics, Geosystems*, *20*(7), 3268–3288. https://doi.org/10.1029/2019gc008334

Villey, M., Le Metour, J., & De Gramont, X. (1986). *Geological map of Fanjah*. Muscat, Oman: Ministry of Petroleum and Minerals, Directorate General of Minerals, Sultanate of Oman.

Warren, C. J., Parrish, R. R., Waters, D. J., & Searle, M. P. (2005). Dating the geologic history of Oman's Semail ophiolite: Insights from U-Pb geochronology. *Contributions to Mineralogy and Petrology*, *150*(4), 403–422. https://doi.org/10.1007/s00410-005-0028-5

Weyhenmeyer, C. E. (2000). *Origin and evolution of groundwater in the alluvial aquifer of the eastern Batinah Coastal plain, Sultanate of Oman: A hydrogeochemical approach*. Bern, CH: University of Bern.

Wilde, A., Simpson, L., & Hanna, S. (2002). Preliminary study of Tertiary hydrothermal alteration and platinum deposition in the Oman ophiolite. *Journal of the Virtual Explorer*, *6*, 7–13.

Wilson, C. R., Spiegelman, M., van Keken, P. E., & Hacker, B. R. (2014). Fluid flow in subduction zones: The role of solid rheology and compaction pressure. *Earth and Planetary Science Letters*, *401*, 261–274. https://doi.org/10.1016/j.epsl.2014.05.052

Wohlwend, S., Celestino, R., Reháková, D., Huck, S., & Weissert, H. (2017). Late Jurassic to Cretaceous evolution of the eastern Tethyan Hawasina basin (Oman Mountains). *Sedimentology*, *64*(1), 87–110. https://doi.org/10.1111/sed.12326

Wolery, T. J. (1992). *EQ3/6, a software package for geochemical modeling of aqueous systems: Package overview and installation guide (version 7.0) (No. UCRL-MA-110662-PT. 1)*. Lawrence Livermore National Lab.

Wolfe, M. R., & Stockli, D. F. (2010). Zircon (U-Th)/He thermochronometry in the KTB drill hole, Germany, and its implications for bulk He diffusion kinetics in zircon. *Earth and Planetary Science Letters*, *295*(1–2), 69–82. https://doi.org/10.1016/j.epsl.2010.03.025

Wyns, R., Bechennec, F., Le Meteour, J., Roger, J. (1992). *Geological map of the Tiwi Quadrangle, Sultanate of Oman. Geoscience map, scale 1:100,000, Sheet NF 40-8B*. Muscat, Oman: Ministry of Petroleum and Minerals, Directorate General of Minerals, Sultanate of Oman.

Yoshikawa, M., Python, M., Tamura, A., Arai, S., Takazawa, E., Shibata, T., et al. (2015). Melt extraction and metasomatism recorded in basal peridotites above the metamorphic sole of the northern Fizh massif, Oman ophiolite. *Tectonophysics*, *650*, 53–64. https://doi.org/10.1016/j.tecto.2014.12.004

Zarrinkoub, M. H., Amini, S., Aftabi, A., & Karimpour, M. H. (2005). Mineralogy, geochemistry, structural position and a genetic model for listvenite in the east of Iran. *Iranian Journal of Crystallography and Mineralogy*, *13*, 363–378.

Zimmer, K., Zhang, Y., Lu, P., Chen, Y., Zhang, G., Dalkilic, M., & Zhu, C. (2016). SUPCRTBL: A revised and extended thermodynamic dataset and software package of SUPCRT92. *Computers & Geosciences*, *90*, 97–111. https://doi.org/10.1016/j.cageo.2016.02.013